ChemPubSoc Europe

DOI: 10.1002/cmdc.201300429

VIP

Time-Dependent Diaryl Ether Inhibitors of InhA: Structure–Activity Relationship Studies of Enzyme Inhibition, Antibacterial Activity, and in vivo Efficacy

Pan Pan,[a] Susan E. Knudson,[b] Gopal R. Bommineni,[a] Huei-Jiun Li,[a] Cheng-Tsung Lai,[a, c] Nina Liu,[a] Miguel Garcia-Diaz,[d] Carlos Simmerling,[a] Sachindra S. Patil,[e] Richard A. Slayden,*[b] and Peter J. Tonge*[a, c]

The diaryl ethers are a novel class of antituberculosis drug candidates that inhibit InhA, the enoyl-ACP reductase involved in the fatty acid biosynthesis (FASII) pathway, and have antibacterial activity against both drug-sensitive and drug-resistant strains of *Mycobacterium tuberculosis*. In the present work, we demonstrate that two time-dependent B-ring modified diaryl ether InhA inhibitors have antibacterial activity in a mouse model of TB infection when delivered by intraperitoneal injection. We propose that the efficacy of these compounds is related to their residence time on the enzyme, and to identify structural features that modulate drug–target residence time in this system, we have explored the inhibition of InhA by a series of B-ring modified analogues. Seven *ortho*-substituted compounds were found to be time-dependent inhibitors of InhA, where the slow step leading to the final enzyme–inhibitor complex (EI*) is thought to correlate with closure and ordering of the InhA substrate binding loop. A detailed mechanistic understanding of the molecular basis for residence time in this system will facilitate the development of InhA inhibitors with improved in vivo activity.

Introduction

Tuberculosis (TB) is a global infectious disease that is a serious threat to human health due to emergence of multidrug-resistant (MDR-TB) and extensively drug-resistant (XDR-TB) strains of *Mycobacterium tuberculosis*.[1] In 2008, 22% of new TB cases were reported to be MDR-TB,[2] however, there is a current lack of new TB-specific chemotherapeutics to combat the spread of these resistant organisms. In the search for novel TB lead candidates, we and others have developed inhibitors of InhA, the enoyl-ACP reductase involved in the *M. tuberculosis* fatty acid biosynthesis (FASII) pathway.[3] InhA plays an essential role in cell viability and is a target for the TB drug isoniazid (INH).[4] Since resistance to INH results primarily from defects in drug activation and not from mutations in InhA,[5] compounds that directly inhibit InhA should be active against INH-resistant strains. Based on this premise, we developed a series of diaryl ethers (Figure 1) that are potent inhibitors of InhA and that have antimicrobial activity against both INH-sensitive and resistant strains of *M. tuberculosis*.[3a] Unfortunately, a previous study demonstrated that **PT004** (Figure 1b) had efficacy in a macrophage TB assay but did not show efficacy in the rapid murine model of TB infection.[6] Our studies on the enoyl-ACP reductase enzymes in other pathogens revealed that the in vivo efficacy of diaryl ether inhibitors correlates with their residence time (t_R) on the enzyme target ($t_R = 1/k_{off}$) but not with their binding affinities (K_i) values for enzyme inhibition or their in vitro antibacterial activity (i.e., the minimum inhibitory concentration; MIC).[7] Since K_i and MIC values are determined at constant drug concentration, the studies support the importance of drug-target residence time in determining in vivo drug activity given that the in vivo drug concentration is not constant.[8] Based on this hypothesis, we developed long residence time inhibitors of InhA and discovered **PT070**,[9] the first slow-onset diaryl ether inhibitor, which showed a 430-fold increase in binding affinity to InhA compared with **PT004** (Figure 1b). **PT070** has a residence time of 24 min on InhA and binds to the enzyme through a two-step induced-fit mechanism, in which the rapid formation of the initial EI complex is followed by the slow formation of the final enzyme–inhibitor complex (EI*) (Figure 2).

[a] Dr. P. Pan, Dr. G. R. Bommineni, Dr. H.-J. Li, C.-T. Lai, Dr. N. Liu, Prof. C. Simmerling, Prof. P. J. Tonge
Institute for Chemical Biology & Drug Discovery
Department of Chemistry, Stony Brook University
Stony Brook, NY 11794-3400 (USA)
E-mail: peter.tonge@sunysb.edu

[b] Dr. S. E. Knudson, Prof. R. A. Slayden
Department of Microbiology, Immunology & Pathology
Colorado State University
1619 Campus Delivery, Fort Collins, CO 80523-2025 (USA)
E-mail: richard.slayden@colostate.edu

[c] C.-T. Lai, Prof. P. J. Tonge
Biochemistry & Structural Biology, Stony Brook University
Stony Brook, NY 11794-3400 (USA)

[d] Prof. M. Garcia-Diaz
Pharmacological Sciences Graduate Program, Stony Brook University
Stony Brook, NY 11794-3400 (USA)

[e] Dr. S. S. Patil
Kanashi Biotech Pvt Ltd, A-27 H Block MIDC, Pimpri, Pune 411018 (India)

Supporting information for this article is available on the WWW under http://dx.doi.org/10.1002/cmdc.201300429.

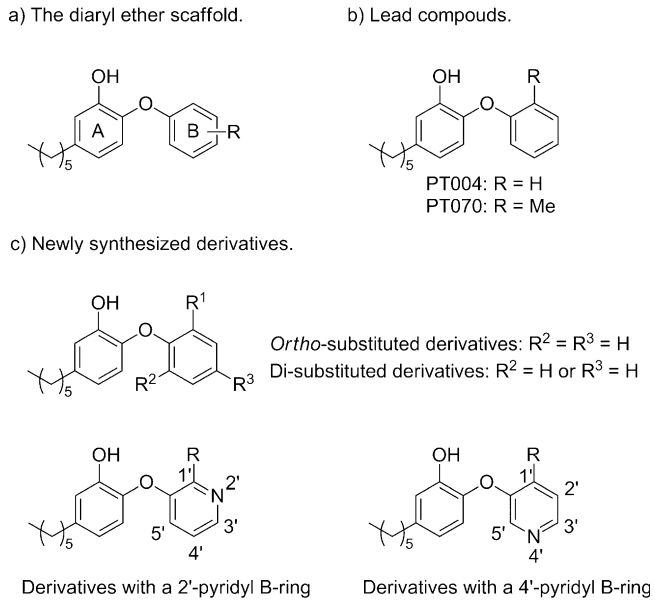

Figure 1. a) The general structure of the diaryl ether scaffold. The diaryl ethers share a scaffold consisting of an alkyl phenol A-ring and a B-ring with various substituents. b) Lead compounds for structure–activity relationship studies described here. c) Newly synthesized derivatives including *ortho*-substituted derivatives, di-substituted derivatives, and derivatives with heterocyclic B-rings (2′-pyridyl or 4′-pyridyl).

In order to further rationally modulate residence time in this system, we need to understand the molecular basis that governs the interconversion of EI and EI*. The structural change that occurs between EI and EI* has been linked to motions of the substrate binding loop (residues 198–208), which closes over the active site when the inhibitor is bound.[9] Based on the premise that substituents on the B-ring of the diaryl ether play a critical role in the energetics of the EI to EI* transition, we now report structure–activity relationship (SAR) studies on a series of B-ring-modified diaryl ethers that provide insight into the role of specific interactions between the inhibitor and the substrate binding loop in the time-dependent inhibition of InhA. In addition, to further substantiate the link between residence time and in vivo antibacterial activity, we have determined the efficacy of **PT070** in a mouse model of TB infection together with that of an additional time-dependent InhA inhibitor, **PT091**.

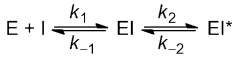

Figure 2. Kinetic scheme for time-dependent inhibition. The time-dependent diaryl ether inhibitors bind through a two-step induced-fit mechanism in which the rapid formation of the initial enzyme–inhibitor complex (EI) is followed by a slow step leading to the final enzyme–inhibitor complex (EI*).

Chemistry

Previous approaches to the preparation of diaryl ethers by us involved a Buchwald–Hartwig cross-coupling to link the A-ring and B-ring, and the attachment of an alkyl group using Negishi coupling (Scheme 1).[3a,10] This synthetic route employed air- and moisture-sensitive catalysts, and resulted in low overall yields (10–20%). To streamline this process, we established a new route in which intermediate **3** was prepared from vanillin (Scheme 2). This involved protection of the vanillin hydroxy with a benzyl group, attachment of a pentenyl group using a Wittig reaction, hydrogenation to reduce the double bond, and subsequent cleavage of the protecting group. Once compound **3** was obtained, a variety of aromatic groups were coupled to the phenol to provide intermediates for the target molecules (Scheme 3–8).

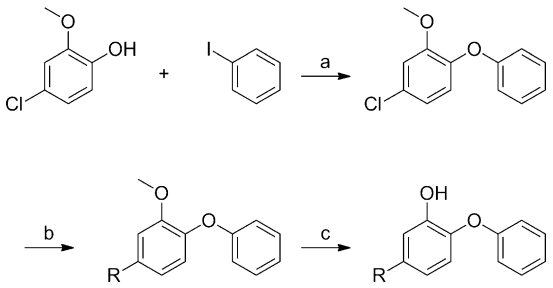

Scheme 1. Previously reported synthesis of diaryl ethers.[3a] *Reagents and conditions*: a) $(CuOTf)_2$·PhH, Cs_2CO_3, EtOAc, $[ArCO_2H]$, toluene, 110 °C; b) RZnCl, $Pd(P(tBu)_3)_2$,THF/NMP (1:10), 130 °C; c) BBr_3, CH_2Cl_2, −78 °C.

Although additional steps were employed in this new approach, the overall yield of **PT092**, which has a similar structure to previously reported diaryl ethers, was 37% (Scheme 4). For simple aryl halides, the reported copper(I) iodide-catalyzed coupling reactions[11] are generally useful for the synthesis of aryl ethers, such as compound **4**. However, this method is limited by reactivity and steric hindrance of the aryl halide, whereas the recently published air-stable copper(I) bipyridyl complex[12] showed higher catalytic efficiency and afforded more

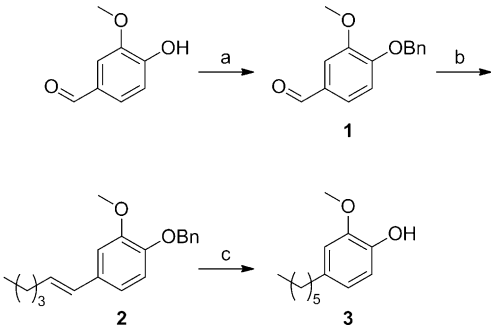

Scheme 2. Synthesis of intermediate **3**. *Reagents and conditions*: a) BnBr, aq KOH, MeOH, reflux, 2 h, 91%; b) $nC_5H_{11}PPh_3Br$, *n*BuLi, THF, −78 °C→RT, 2.5 h, 82%; c) H_2, Pd/C, EtOH, 6 h, 89%.

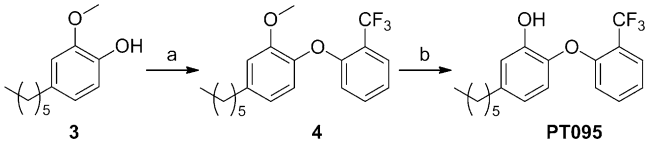

Scheme 3. Synthesis of **PT095**. *Reagents and conditions*: a) 1-iodo-2-(trifluoromethyl)benzene, $(CuOTf)_2$·PhH, Cs_2CO_3, 1-naphthoic acid, EtOAc, toluene, 110 °C, 24 h, 75%; b) BBr_3, CH_2Cl_2, −78 °C→RT, 3 h, 88%.

complex biaryl coupled products, such as compound **28**. We also modified the Ullmann protocol to use the nucleophilic aromatic substitution reaction with fluoronitrobenzenes,[10,13] benzonitriles, picolinonitrile, pyridine *N*-oxide,[14] or isonicotinonitrile to afford the aryl ethers **5**, **15**–**18**, **27**, **29**, **31**, **33**, **34**, **36**,

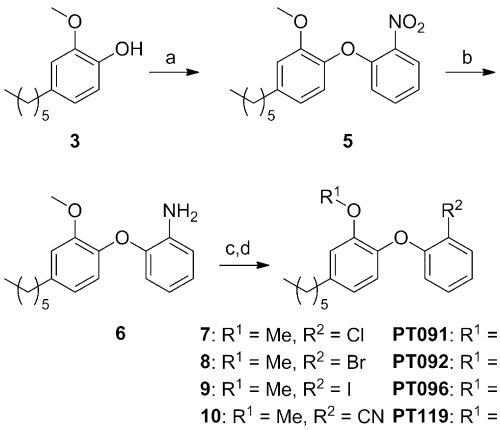

Scheme 4. Derivatives with mono-substituted B-rings. *Reagents and conditions*: a) K_2CO_3, 1-fluoro-2-nitrobenzene, 18-crown-6, DMF, 110 °C, 3 h, 66%; b) H_2, Pd/C, EtOH, 6 h, 91%; c) $NaNO_2$, AcOH, H_2O, CuX, 0 °C, 30 min; d) BBr_3, CH_2Cl_2, −78 °C→RT, 5 h.

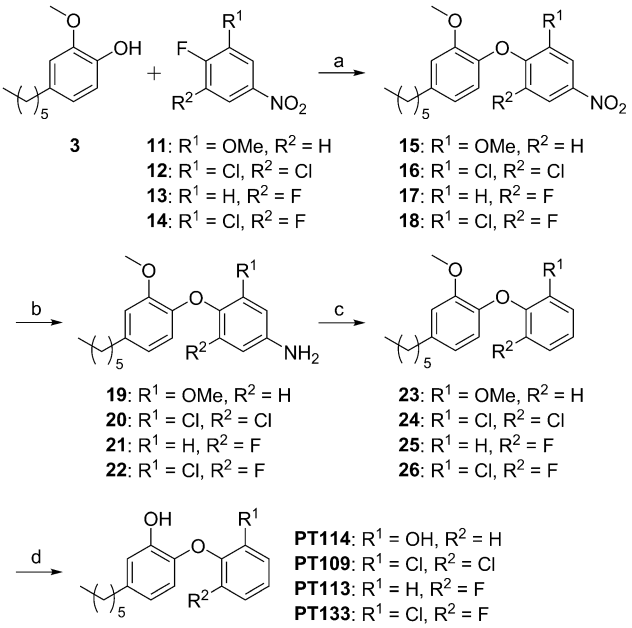

Scheme 5. Derivatives with various B-rings. *Reagents and conditions*: a) K_2CO_3, DMAc, 160 °C, 3 h; b) Zn, HCl, EtOH/H_2O (10:1), 0 °C→RT, 1 h; c) $NaNO_2$, H_2SO_4, Zn, EtOH/H_2O (10:1), 0 °C→reflux, 3 h; d) BBr_3, CH_2Cl_2, −78 °C→RT, 5 h.

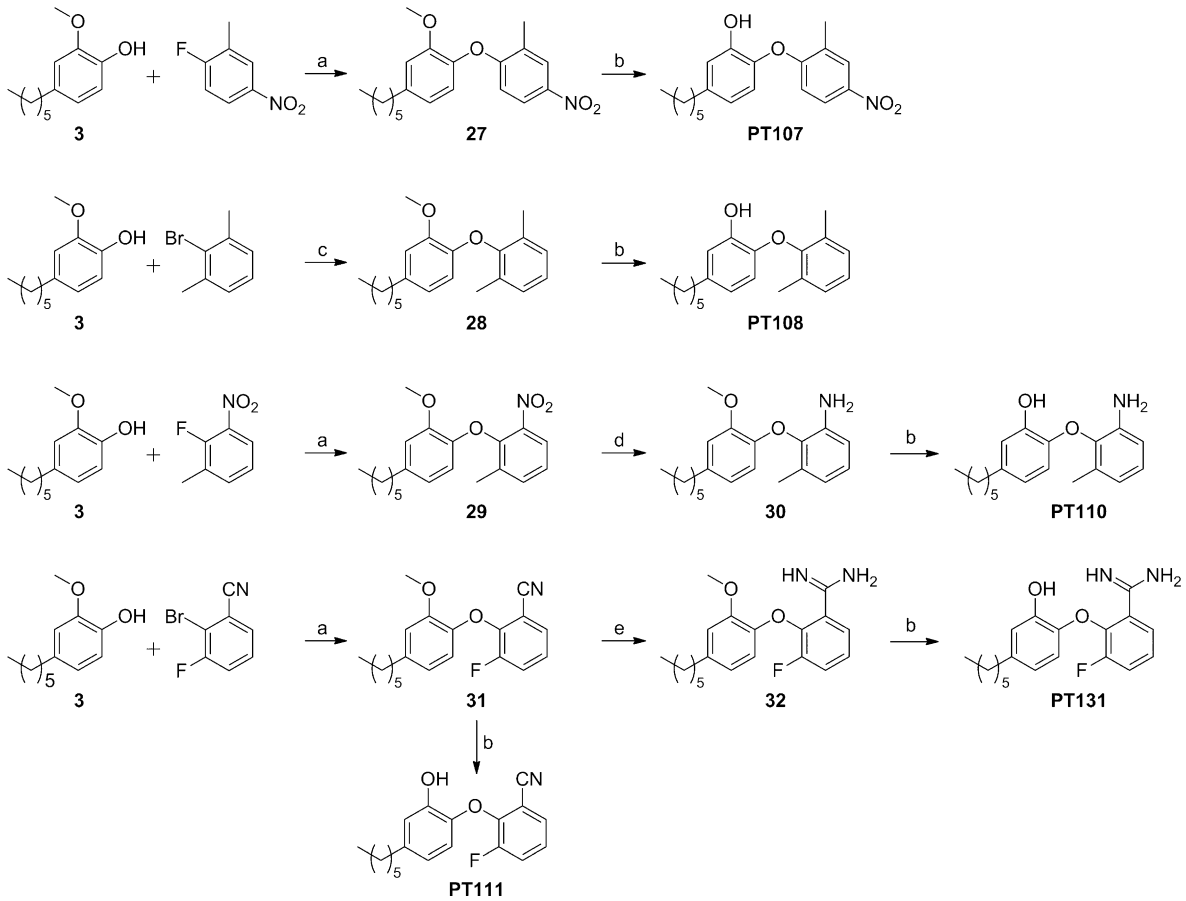

Scheme 6. Derivatives with di-substituted B-rings. *Reagents and conditions*: a) K_2CO_3, DMAc, 160 °C, 4 h; b) BBr_3,CH_2Cl_2, −78 °C→RT, 3 h; c) K_3PO_4,$Cu(bipy)_2BF_4$, 120 °C, DMF, 48 h, 10%; d) Zn, HCl, 0 °C→RT, 1 h, 41%; e) $Li(TMS)_2$, THF, 0 °C→RT, 3 h, 46%.

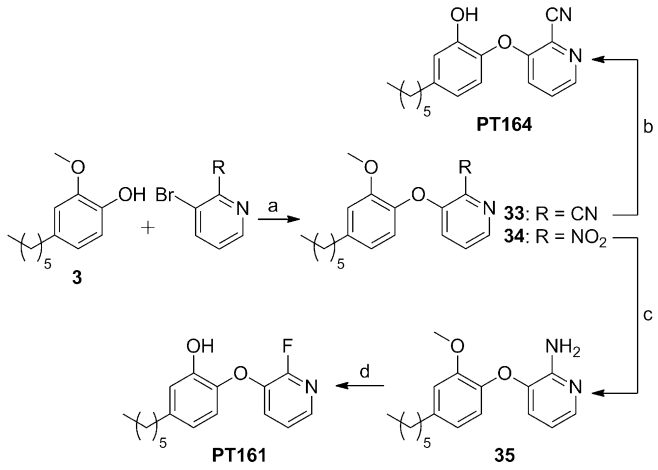

Scheme 7. Derivatives with 2′-*N*-pyridyl B-rings. *Reagents and conditions*: a) Cs_2CO_3, MeCN, 80 °C, 2 h; b) BBr_3, CH_2Cl_2, −78 °C→RT, 2 h; c) Fe, AcOH/H_2O (4:1), 100 °C, 30 min, 77%; d) 1. 70% HF in pyridine, 0–60 °C, 1 h; 2. BBr_3, CH_2Cl_2, −78 °C→RT, 2 h, 49%.

and **38**. The ether intermediates were transformed into the appropriately substituted diaryl ethers **6**, **19**–**26**, **30**, **32**, **35**, **37**, and **39** using group conversions such as reductions, deaminations,[13,15] diazotizations, hydrolysis, and fluorination. Final compounds were obtained after the subsequent demethylation reaction with boron tribromide.[13,15a,c]

The synthesis of **PT134** is challenging. It was first attempted by using several metal-catalyzed coupling conditions[11,12] to link compound **3** with *tert*-butyloxycarbonyl (Boc)-protected 5-bromopyrimidin-4-ylamine, however, none of these conditions afforded the desired product. To address this hurdle, we constructed the pyrimidine ring using a five-step synthesis that employs relatively simple reaction conditions (Scheme 9). The alkylation of **3** with ethyl bromoacetate provided **40**, which was then subjected to formylation followed by condensation to give **41**. Conversion of the hydroxy to a chloro group using phosphoryl chloride and nucleophilic substitution by ammonia at 130 °C provided **43**, which was subsequently demethylated using boron tribromide to give the final product **PT134**.

Results and Discussion

We previously described the synthesis of a series of diphenyl ether inhibitors of InhA, the most potent of which had hexyl or octyl substituents on the inhibitor A-ring ($K_i' = 9.4$ and 1.1 nM, respectively).[3a] We evaluated the pharmacodynamic properties of the hexyl analogue (**PT004**) in a mouse model of TB infection, but failed to observe a significant decrease in bacterial load.[6] Pharmacokinetic analysis of **PT004** suggested that improvements in C log *P* might result in improved in vivo activity, and we subsequently synthesized a series of B-ring substituted **PT004** analogues.[10] These studies, coupled with additional SAR data on the inhibition of the enoyl-ACP reductase in other organisms,[16] indicated that modification to the

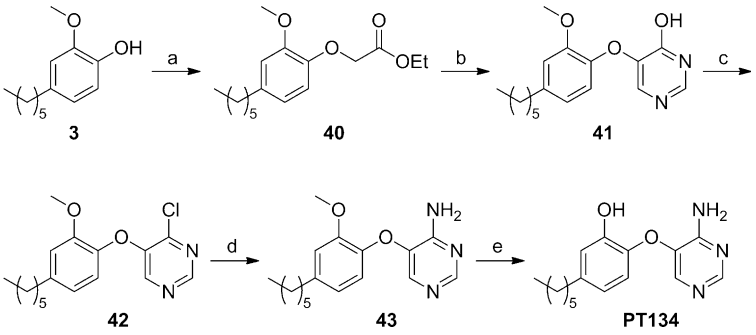

Scheme 9. Derivatives with a pyrimidyl B-ring. *Reagents and conditions*: a) ethyl bromoacetate, NaOEt, EtOH, 80 °C, 16 h, 35%; b) 1. ethyl formate, NaH, THF, 65 °C, 4 h; 2. formamidine acetate, EtOH/MeOH (1:1), 80 °C, 4 h, 47%; c) $POCl_3$, 70 °C, 3 h, 46%; d) NH_4OH, 130 °C, 18 h, 87%; e) BBr_3, CH_2Cl_2, −78 °C→RT, 3 h, 68%.

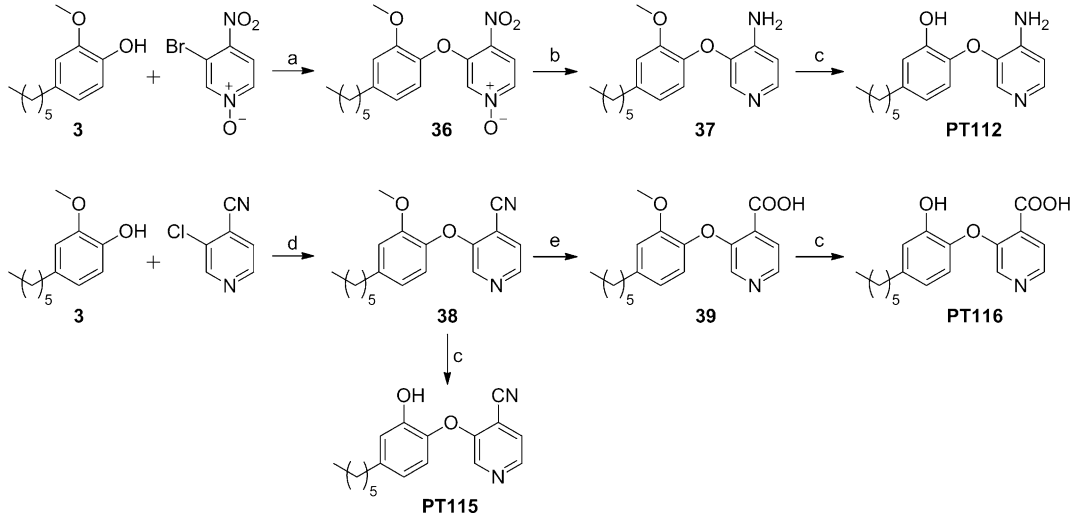

Scheme 8. Derivatives with 4′-*N*-pyridyl B-rings. *Reagents and conditions*: a) NaOH, MeCN, 80 °C, 2 h, 60%; b) Fe, AcOH, H_2O, 80 °C, 2 h, 57%; c) BBr_3, CH_2Cl_2, −78 °C→RT, 5 h; d) K_2CO_3, DMAc, 160 °C, 7 h, 69%; e) KOH, MeOH, 80 °C, 2 h, 82%.

B-ring might also further improve the affinity of this inhibitor series for InhA, leading to the synthesis of an *ortho*-methyl-substituted analogue with significantly improved affinity for InhA (**PT070**).[9] **PT070** was found to be slow-onset inhibitor of InhA with a residence time of 24 min on the enzyme. Based on the knowledge that drug–target residence time could have a dramatic impact on in vivo drug activity,[8a,b,f] we set out to explore the effect of B-ring substituents on the time-dependent inhibition of InhA and on in vivo activity. We show here that time-dependent inhibition is sensitive to the substitution pattern. We also show that **PT070**, together with an analogue bearing an *ortho*-chloro group (**PT091**) decrease bacterial load in the spleens of mice infected with *M. tuberculosis*.

Table 1. Derivatives with *ortho*-substituent groups.

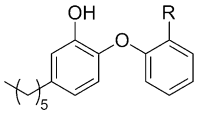

Compd	R	IC_{50}[a] [nM]	MIC[e] [μg mL^{-1}]	K_i [nM]	Slow onset?	t_R [min]
PT004	H	11 ± 1[b]	2.1	9.4 ± 0.5	No	–
PT010	NO_2	182 ± 2.0[c]	12.50	N.D.	Yes	27 ± 6
PT013	NH_2	61.9 ± 4.5[c]	3.13	N.D.	No	–
PT070	CH_3	50.7 ± 4[c]	3.125	0.044 ± 0.005	Yes	24 ± 2
PT091	Cl	49.5 ± 2.2[c]	1.56	0.96 ± 0.14	Yes	21 ± 3
PT092	Br	10.0 ± 0.8[d]	3.125	0.20 ± 0.05	Yes	30 ± 3
PT095	CF_3	29.7 ± 1.2[d]	50.00	N.D.	No	–
PT096	I	44.6 ± 7.5[c]	25	3.72 ± 5.13	No	–
PT113	F	12.1 ± 4.8[d]	1.56	0.09 ± 0.02	Yes	9 ± 3
PT114	OH	48 ± 3[c]	12.5	15.9 ± 3.7	No	–
PT119	CN	235.6 ± 10.0[c]	2.5	2.14 ± 0.35	Yes	80 ± 12

[a] The half maximal inhibitory concentration (IC_{50}) is defined as the inhibitor concentration required for 50% inhibition of enzyme activity. IC_{50} values were determined at an enzyme concentration of [b] 1 nM, [c] 100 nM and [d] 20 nM. [e] The minimum inhibitory concentration (MIC) is the lowest inhibitor concentration required to inhibit visible growth of bacteria. MIC values are the mean of three independent experiments. IC_{50}, K_i, and residence time (t_R) values are the mean ± standard deviation of three independent experiments. N.D. = not determined.

Ortho-substituted diaryl ethers

Compounds **PT004**,[3a] **PT010**,[10] **PT013**,[10] and **PT070**[9] have been reported in previous SAR studies. The improvement in binding affinity of **PT070** for InhA compared with **PT004** is thought to result from decreased freedom of rotation about the ether bond, together with increased hydrophobic contacts between the B-ring and A198, M199, I202, and V203 in the substrate binding loop based on the structural data.[9] Introduction of an *ortho*-methyl group on the B-ring also resulted in an additional interaction between the inhibitor and A198. These increased contacts are thought to be critical for the formation of the EI* complex in which helix-6 of the substrate binding loop has closed over the active site.[9,17] Replacement of the methyl group with an amino group resulted in an analogue with similar IC_{50} and MIC values, but slow-onset inhibition was not detected for this compound, supporting the importance of B-ring *ortho*-substitution for time-dependent inhibition. Consequently, to better understand the mechanism of the time-dependent kinetics and further modulate the residence time, analogues with various *ortho* substituents were designed and synthesized (Table 1).

Compared with **PT070**, compounds **PT113** (F), **PT091** (Cl), and **PT092** (Br) all have sub-nanomolar K_i values with similar or shorter residence times. In contrast, under the assay conditions employed, the only analogue with a longer residence time, **PT119** (t_R = 80 min), had a binding affinity that is decreased by approximately 50-fold compared with **PT070**.

In an attempt to rationalize these observations, we determined the crystal structures of InhA bound to **PT092**[17] and **PT119** (Figures 3 and 4). These compounds form a ternary complex with the enzyme and the oxidized cofactor (NAD^+), and in both ternary complexes, the substrate binding loop of InhA forms an α-helix that closely interacts with the B-ring, similar to the enzyme–inhibitor complexes formed by other time-dependent inhibitors.[9,17,18] This is in contrast to the structures of complexes formed with rapid reversible inhibitors in which the substrate binding loop is either disordered[3a] or forms an α-helix in a much more open conformation.[17] The re-

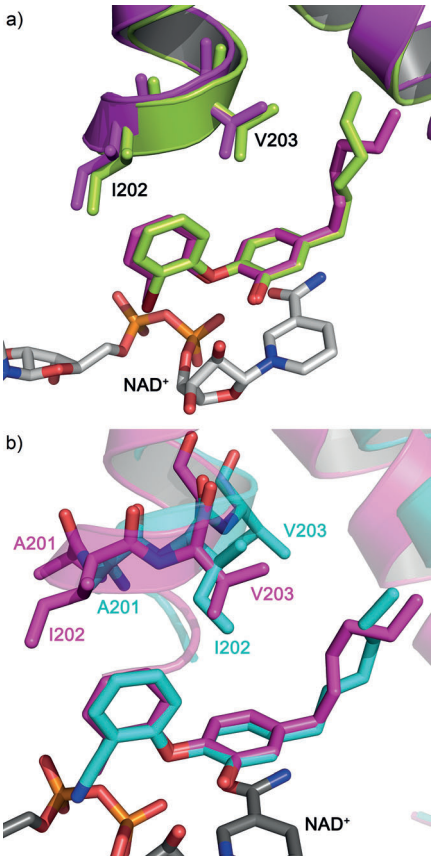

Figure 3. Superimposed structures of InhA complexes involving **PT070**, **PT092** and **PT119**. a) Overlay of **PT070** (magenta; PDB: 2X23) and **PT092** (lime; PDB: 4OHU) bound to InhA. b) Overlay of **PT070** (magenta; PDB: 2X23) and **PT119** (cyan; PDB: 4OIM) bound to InhA. The graphics were generated using PyMol.[34]

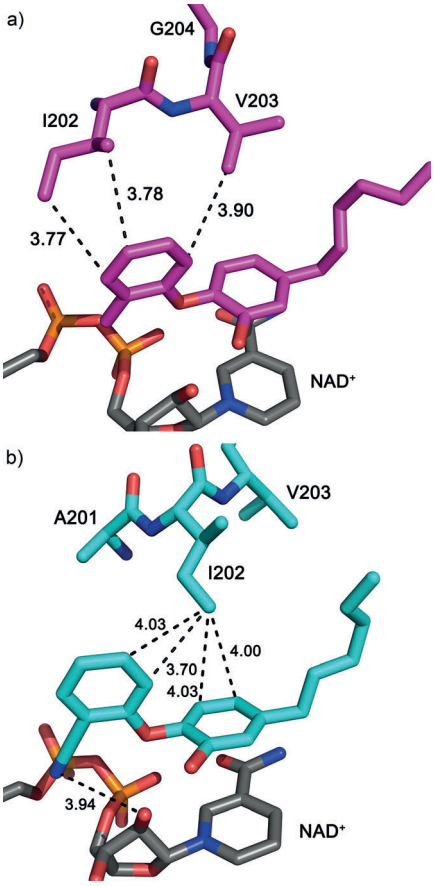

Figure 4. Interactions in the **PT070** and **PT119** enzyme–inhibitor complexes. a) Hydrophobic interactions between the **PT070** B-ring and the substrate binding loop (magenta; PDB: 2X23). b) Hydrophobic and hydrogen-bonding interactions of the **PT119** B-ring with the substrate binding loop and cofactor (cyan; PDB: 4OIM). The graphics were generated using PyMol.[34]

sults support the correlation between slow-onset inhibition and ordering coupled to closure of the substrate binding loop previously suggested for the FabI class of enoyl-ACP reductases.[19]

The substrate binding loop in the **PT092** complex exhibits a very similar conformation to that observed in the **PT070** complex (Figure 3a), which is expected from their similar residence times and binding affinities. However, in one of the four subunits in the asymmetric unit, a different binding mode of **PT092** relative to helix-6 is observed: A201 and I202, instead of I202 and V203, make van der Waals contacts with the inhibitor, which is accompanied by a twist of the helix-6 backbone and displacement of the adjacent helix-7. Interestingly, the altered position of the substrate binding loop in this InhA–**PT092** subunit is found exclusively in the structure of **PT119** bound to InhA (Figures 3b and 4b). We speculate that this altered helix-6 conformation rationalizes the increase in residence time of **PT119** ($t_R = 80$ min) relative to **PT070** ($t_R = 24$ min) and propose that replacement of the B-ring methyl group with a cyano group raises the energy barrier between EI and EI* on the binding reaction coordinate.

Owing to the crystallization conditions and the potential impact from crystal packing, the observed structure for the **PT119** complex could represent a snapshot along the binding coordinate from EI to EI*. Nevertheless, the decreased overall binding affinity of **PT119** compared with **PT070** indicates that EI* for **PT119** is destabilized relative to **PT070**. Since the overall energy barrier between EI and EI* has increased for **PT119**, it follows that the transition state between EI and EI* is even more destabilized ($\Delta\Delta G^{TS} > \Delta\Delta G^{EI*}$) (Figure 5). In the crystal structure, **PT119** appears to make reduced van der Waals contacts with helix-6 residues (Figure 4). In addition, the bulkier cyano substituent approaches the adjacent NAD and InhA backbone within an unfavorably distance of 3.4 Å. These less than optimal interactions provide a plausible explanation for the proposed destabilization.

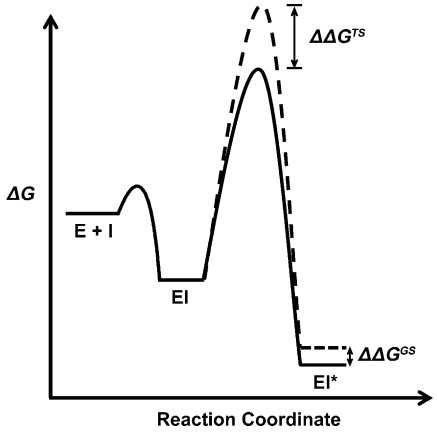

Figure 5. Free energy diagram for the interaction of **PT070** (——) and **PT119** (-----) with InhA. These inhibitors bind through a two-step mechanism in which the energy barrier between enzyme–inhibitor complex (EI) and final enzyme–inhibitor complex (EI*) is assumed to control the rate of formation and breakdown of EI*.

The results of the binding studies are consistent with a previous proposal that B-ring substituents should generally be small in order to be accommodated in the InhA active site.[10] However, here we observe that binding affinity is even more sensitive to substituent size than we originally recognized. In particular, introduction of trifluoromethyl or cyano groups into the *ortho* position of the B-ring resulted in compounds with 50–100-fold weaker binding affinities compared with **PT070**, while the introduction of polar groups such as a hydroxy (**PT114**) also had a significant effect on the binding kinetics, which indicates that hydrophobic interactions between the *ortho* group and the protein are critical. Further studies with compounds containing *ortho* halogens showed no correlation between the binding affinity and electronegativity. These results confirm that a small (containing one or two heavy atoms) *ortho* substituent is necessary for high-affinity binding and that this group should not be a hydrogen-bond donor.

Derivatives with di-substituted B-rings

One hypothesis for the improved binding affinity of **PT070** compared with **PT004** is that the additional methyl group restricts rotations around the ether linkage and stabilizes the

Table 2. Derivatives with di-substituted B-ring.

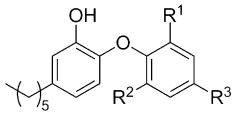

Compd	R^1	R^2	R^3	IC_{50}[a] [nM]	MIC[b] [μg mL^{-1}]	K_i [nM]
PT004	H	H	H	11 ± 1	2.1 ± 0.9	9.4 ± 0.5
PT070	CH_3	H	H	50.7 ± 4	3.125	0.044 ± 0.005
PT107	CH_3	H	NO_2	50 ± 5	6.25	0.13 ± 0.03
PT108	CH_3	CH_3	H	1570 ± 200	100	N.D.
PT109	Cl	Cl	H	86 ± 6	25	N.D.
PT110	CH_3	NH_2	H	N.I.	> 100	N.D.
PT111	F	CN	H	100 ± 9	25	N.D.
PT131	$C(NH)NH_2$	F	H	N.I.	N.D.	N.D.
PT133	F	Cl	H	79.7 ± 24.4	25	N.D.

[a] The half maximal inhibitory concentration (IC_{50}) is defined as the inhibitor concentration required for 50% inhibition of enzyme activity. IC_{50} values were determined at an enzyme concentration of 1 nM. N.I. = no inhibition observed at 2000 nM. [b] The minimum inhibitory concentration (MIC) is the lowest inhibitor concentration required to inhibit visible growth of bacteria. MIC values are the mean of three independent experiments. IC_{50} and K_i values are the mean ± standard deviation of three independent experiments. N.D. = not determined.

conformation observed in the structure of the diphenyl ether bound to the enzyme.[9] Consequently, a series of di-*ortho*-substituted B-ring analogues were designed with two groups *ortho* to the ether bond (Table 2). If hindered rotation about the ether bond is important for binding, these compounds are expected to have increased affinity compared with the analogues with a single *ortho* substituent (Table 1). The two *ortho* groups were chosen from the most potent compounds identified in Table 1, and included methyl, halogen, and cyano groups. Compound **PT107**, an analogue of **PT070**, was also synthesized to examine the tolerance for an additional *para* group.

Unfortunately, none of these derivatives had improved activity compared with their parent compounds (Table 2). To rationalize these results, the docked structure of the dichloro analogue **PT109** was compared with the corresponding docked structure of **PT091** (monochloro) bound to the active site of InhA (Figure 6). This analysis demonstrated that **PT109** has a higher Grid score, van der Waals, and internal energy than **PT091**, which explains the decreased binding affinity of this analogue for the enzyme (Table S1 in the Supporting Information). The extra steric hindrance has resulted in unfavorable van der Waals interactions and thus lowered the binding affinity of the inhibitor.

Enzyme inhibition and antibacterial growth assays revealed that the compounds have similar SAR to compounds with *ortho*-substituted B-rings—protic or large groups are not tolerated at the *ortho* position of the B-ring. Replacing a methyl group in **PT108** with an amino group (**PT110**) resulted in a total loss of binding affinity and inhibition of bacterial growth. Introduction of the large carbamimidoyl pharmacophore (**PT131**) also led to a total loss of inhibitory activity, compared with smaller groups such as cyano or chloro (**PT111** and **PT133**, respectively). Thus, substituents that include halogen or cyano groups are preferred. Although MIC values for the di-*ortho* analogues are raised by 4–15-fold compared with **PT070**, the *ortho*,*para*-disubstituted B-ring analogue **PT107** has similar IC_{50} and MIC values, implying that small *para* groups on the B-ring are well tolerated.

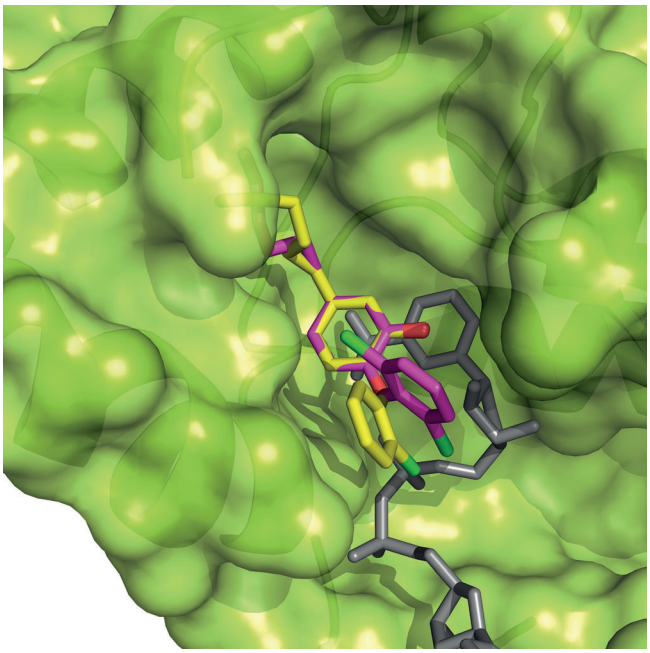

Figure 6. Superimposed modelled structures of InhA complexes involving **PT091** and **PT109**. **PT091** (yellow) and **PT109** (magenta) were docked into the InhA active site (lime) as described in the text. Also shown is the NAD^+ cofactor (gray). The graphic was generated with PyMol.[34]

Derivatives with heterocyclic B-rings

In order to improve hydrophilicity of the diaryl ethers, we also explored analogues with pyridyl B-rings. Previous studies showed that although introduction of an *ortho* nitrogen atom into the B-ring decreased activity significantly, *para* and *meta* nitrogen atoms were well tolerated.[10] However, the position of the *meta* nitrogen is ambiguous on the unsubstituted B-ring. To differentiate 2′- and 4′-N (Figure 1c), 1′-substituted pyridyl derivatives were synthesized and evaluated (Table 3). The substituents included fluoro and cyano groups, which were found to be preferred in studies with the phenyl B-ring analogues, together with an amino group. In addition, a carboxylate group was also introduced to explore the effect of an ionizable group on activity. The pyridyl B-rings were found not to alter the preference for specific *ortho* substituents: the fluorine substituent resulted in the compound with the lowest IC_{50} value (**PT161**) within the 2′-pyridyl derivatives, as did the cyano group (**PT115**) within the 4′-pyridyl derivatives. Importantly, introduction of fluoro or cyano groups led to compounds that displayed slow-onset inhibition (**PT164**, **PT161**), in contrast to the parent compound **PT077**, suggesting that

Table 3. Derivatives with heterocyclic B-rings.

Compd		R	IC_{50}[a] [nM]	MIC[b] [μg mL^{-1}]	Slow onset?	t_R [min]
PT077	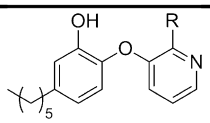	H	190 ± 12	3.13	No	–
PT164		CN	308 ± 4.2	0.313	Yes	N.D.
PT161		F	40 ± 20	0.3125	Yes	N.D.
PT112	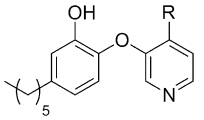	NH_2	69 000 ± 700	50	N.D.	–
PT115		CN	890.6 ± 105.8	12.5	Yes	> 20
PT116		COOH	> 12 000	25	N.D.	–
PT134	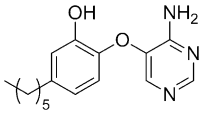		238.8 ± 46.8	3.125	N.D.	–

[a] The half maximal inhibitory concentration (IC_{50}) is defined as the inhibitor concentration required for 50% inhibition of enzyme activity. IC_{50} values were determined at an enzyme concentration of 100 nM. [b] The minimum inhibitory concentration (MIC) is the lowest inhibitor concentration required to inhibit visible growth of bacteria. MIC values are the mean of three independent experiments. IC_{50} and K_i values are the mean ± standard deviation of three independent experiments. N.D. = not determined.

these substituents have an important effect on time-dependent kinetics. Experiments with the carboxylic group (**PT116**) indicated that an ionizable group, presumably bearing a formal negative charge, is not tolerated at the *ortho* position.

We found that in 1′-substituted B-rings, the 2′-N analogues generally had lower MIC and IC_{50} values compared with the 4′-N compounds (**PT164** vs **PT115**). Although the amino group previously resulted a fivefold increase in the IC_{50} value compared with the fluoro group (**PT013** vs **PT113**), this difference increased to 1700-fold (**PT112** vs **PT161**), very likely caused by the different scaffolds. The benefit of the 2′-N atom was also seen in **PT134**, which has both 2′- and 4′-N. Improved IC_{50} and MIC values were observed for **PT134** compared with the corresponding 4′-N analogue **PT112**, which has a 300-fold lower IC_{50} value. The X-ray structure of **PT070** bound to InhA was used to identify potential differences in the interaction of 2′- and 4′-N analogues with the enzyme. This analysis revealed that although the 2′- and 4′-N atoms have similar hydrophobic contacts with I202 and M161, the 2′-N position is able to form additional hydrogen-bonding interactions with the backbone amide of G96 (Figure 7). The poor MIC values for the 4′-pyridyl compounds are consistent with the relatively weak affinities of these inhibitors for InhA, while the 2′-pyridine compounds had MIC values that were generally better than compounds with phenyl B-rings (Table 1) suggesting that the pyridine B-ring may aid uptake into the bacterium.

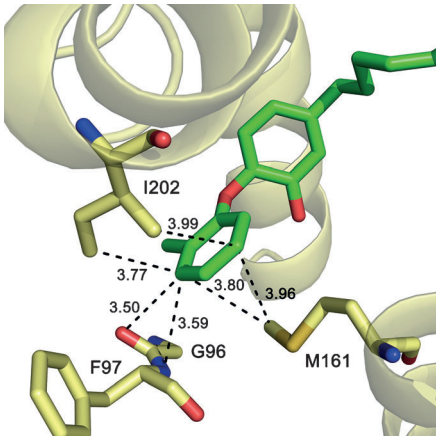

Figure 7. Interactions between the **PT070** B-ring and InhA. Possible hydrophobic and hydrogen-bonding interactions are shown for the 2′- and 4′-positions of the **PT070** (green) B-ring. The graphic was generated from crystal structure 2X23 using PyMol.[34]

Rapid model of in vivo efficacy

PT004 decreased the bacterial load in the rapid macrophage model of TB infection,[6] demonstrating that it is able to enter the macrophage and kill *M. tuberculosis* bacteria under altered growth conditions. However, **PT004** did not significantly decrease the bacterial load in the lung or spleen in the rapid murine model of TB.[6] In the present study, the time-dependent inhibitors **PT070** and **PT091** were evaluated for efficacy when delivered via intraperitoneal injection in the same mouse model.

Compared with untreated controls, **PT070** decreased the bacterial counts in the spleen 0.57 ± 0.26 $\log_{10}$ with a p value of 0.007, while **PT091** decreased the bacterial counts in the spleen 0.69 ± 0.22 $\log_{10}$ with a p value of 0.0002 (Figure 8a). Importantly, the spleen is a secondary site of TB infection, and if a compound can decreased the bacterial burden in the spleen, it is indicative of an ability to control dissemination and disease progression. In contrast, **PT004** is a rapid reversible InhA inhibitor that does not demonstrate efficacy in the murine model of TB. Importantly, **PT070** and **PT091** are slow-onset inhibitors having residence times of 24 and 21 min, respectively. The improved efficacy of diaryl ethers that have increased residence time is consistent with observations in the *Francisella tularensis* infection model,[7] and highlights the potential importance of drug–target residence time for modulating in vivo drug efficacy.[8e,f,20]

Conclusions

Twenty compounds were synthesized based on the diaryl ether scaffold, with a hexyl-substituted A-ring and various modifications to the B-ring. All of the compounds were evaluated for enzyme inhibition of InhA and cell-based antibacterial activity against *M. tuberculosis*. Crystallographic data demonstrated that the slow-onset inhibitors **PT092** and **PT119** resulted in a more ordered and closed InhA substrate binding loop, in agreement with our hypothesis that motions of this loop are related to the structural change that accompanies the EI to EI* transition for slow-onset inhibitors. The relatively large cyano group in **PT119** creates steric hindrance, introduces conformational change of helix-6, and preferentially destabilizes

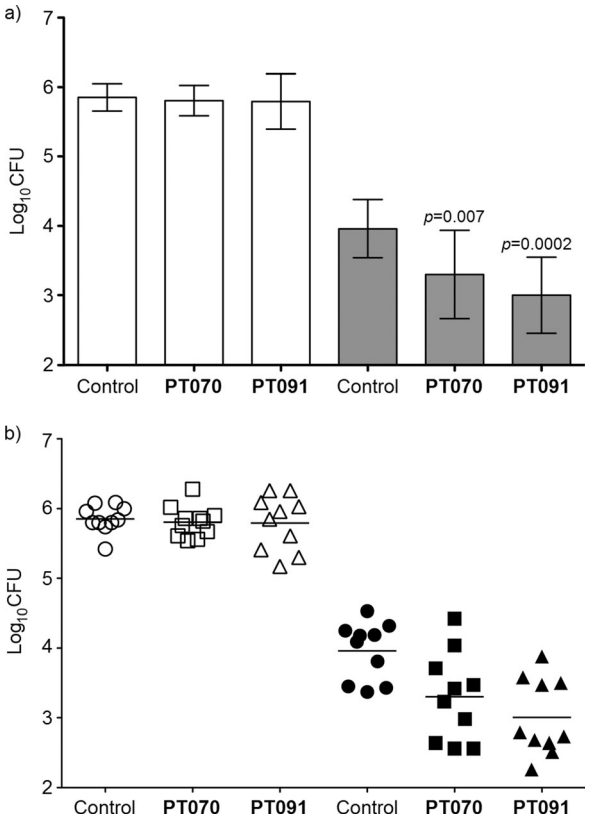

Figure 8. a) Histogram and b) scatterplot of colony-forming unit (CFU) data from the lung and spleen of animals infected with *M. tuberculosis* (Erdman) and either untreated (control) or drug-treated. Open bars or symbols represent CFU data from the lung, whereas shaded bars and symbols represent CFU data from the spleen. All compounds were formulated in 15% EtOH, 20% propylene glycol, 40% polyethylene glycol 400, phosphate-buffered saline and delivered via intraperitoneal injection. Animals were treated with **PT070**, 50 mg kg^{-1} BID Day 2, 25 mg kg^{-1} BID Day 3–10, or with **PT091**, 25 mg kg^{-1} BID Day 1–4, 12.5 mg kg^{-1} BID Day 5–6, 12.5 mg kg^{-1} SID and 25 mg kg^{-1} SID Day 7–10. The significance between control and treatment groups was determined via an unpaired, one-tailed t-test (t-test 1,2) with 95% confidence intervals from mean CFU values for the organs (GraphPad Software version 5, San Diego, USA; http://www.graphpad.com).

the transition state between EI and EI* compared with the EI* ground state, thus resulting in a longer residence time. The activity of the diaryl ether compounds is highly sensitive to the size of the *ortho* substituents on the B-ring. Once the group has more than two heavy atoms, the activity is significantly decreased. In addition, within the acceptable size limits for this group, non-hydrogen bond donors are preferred.

Introduction of groups on both *ortho* positions resulted in a loss of activity that, according to docking studies, leads to a conformation in which there are unfavorable van der Waals interactions with the enzyme. The o*rtho*,*para*-di-substituted compound **PT107** showed similar activity to that of the parent compound, suggesting that *para* groups on the B-ring are well tolerated. We were able to distinguish 2′-N and 4′-N pyridyl B-ring analogues by introducing *ortho* substituents into the B-ring. The 2′-N pyridyl B-rings had significantly better activity than the 4′-N analogues, which may reflect the improvement in cell penetration of these compounds and suggests that the pyridyl B-ring is a better scaffold than the phenyl B-ring.

For all the diaryl ether compounds, slow-onset inhibitors always have higher binding affinity than rapid reversible inhibitors. In contrast to the previously reported lack of efficacy for the rapid onset inhibitor **PT004**, the slow-onset inhibitors **PT070** and **PT091** have demonstrated efficacy in a rapid animal model of TB infection, causing a decrease in bacterial colony-forming units (CFUs) in the spleen. Together, these results support the importance of slow-onset kinetics for in vivo drug efficacy.[16]

Experimental Section

Chemistry

All commercially available chemicals and solvents were used as supplied without further purification. All new compounds gave satisfactory spectroscopic and/or analytical data. ^{1}H and ^{13}C NMR spectra were recorded at 300 or 400 MHz (Varian INOVA), and chemical shifts (δ) are reported in parts per million (ppm) downfield from the internal standard, tetramethylsilane (TMS). Mass spectra (MS) were obtained using electrospray (ES) ionization techniques (Agilent Technologies, 1100 Series LC/MSD). HPLC purification was performed using a controller (Shimadzu CBM-20A), a solvent delivery unit (Shimadzu LC-20A), and a detector (Shimadzu SPD-20A), with a PFP column (Phenomenex lunar, 3.5 μm, 4.6× 100 mm). Compounds were eluted with H_2O/CH_3CN (15:85 at 0 min, 0:100 at 22 min, flow rate: 1.0 mL min^{-1}) and detected at 254 and 278 nm. The purity of all target compounds is >98% as determined by ^{1}H NMR or HPLC.

General procedure of diazotization (for 7, 8, 9, 10): The appropriate aniline (1 mmol) was dissolved in AcOH (10 mL) and H_2O (100 mL), and the solution was cooled to −10 °C. $NaNO_2$ (103.9 mg, 1.5 mmol) was added slowly, followed by the appropriate halide (1.5 mmol) after 30 min. The ice bath was removed, and the reaction was stirred for approximately 2 h. The reaction mixture was then diluted with CH_2Cl_2 (250 mL) and washed with H_2O (150 mL). The organic layer was dried over $MgSO_4$, filtered and concentrated in vacuo to give crude product. The crude compound was purified by column chromatography or used in the next step without purification.

General procedure for the aromatic substitution reaction (for 5, 15, 16, 17, 18, 27, 29, 31, 38): The appropriate nitrobenzene (1.24 mmol), K_2CO_3 (1.03 mmol), and a catalytic amount of 18-crown-6 ether were added to a stirred solution of the corresponding phenol (1.03 mmol) in DMF (3 mL) at RT. The solution was then heated at 110 °C for 3 h. After completion of the reaction, as shown by TLC, the reaction mixture was diluted with water (20 mL) and extracted with EtOAc (2×20 mL). The combined organic phases were washed with brine (30 mL), dried over anhydrous Na_2SO_4, filtered and concentrated in vacuo. The crude product was purified by column chromatography to afford the substituted nitrobenzene.

General procedure for reduction of nitrobenzene to aniline (for 6, 19, 20, 21, 22, 30): Concd HCl (1.3 mL) was added dropwise to a stirred solution of the nitrobenzene (0.78 mmol) in EtOH (15 mL) at 0 °C, and the mixture was stirred for 5 min. Zn powder (17.3 mmol) was then added slowly, and the reaction mixture was allowed to come to RT. The reaction was monitored by TLC, and after completion (~1 h), the reaction was quenched with Et_3N and filtered. The filtrate was concentrated in vacuo, and the crude

product was purified by column chromatography to afford the corresponding aniline.

General procedure for deamination of anilines (for 23, 24, 25, 26): Concd H_2SO_4 (5 mL) was added dropwise to a stirred solution of the aniline (4.3 mmol) in EtOH (25 mL) at 0 °C. A saturated solution of $NaNO_2$ in H_2O (8.6 mmol, 5 mL) was added very slowly, and the reaction mixture was stirred at 0 °C for 30 min. The solution was allowed to come to RT, and then Zn powder (43 mmol) was added. After heating at reflux for 0.5 h, the remaining Zn powder was added, and the mixture was heated at reflux for an additional 2.5 h. After completion of the reaction, the mixture was filtered and neutralized with saturated aq $NaHCO_3$ (pH 7–8). The organic solvent was removed by evaporation in vacuo, and the aqueous solution was then extracted with EtOAc (2×50 mL). The combined organic layers were washed with water (50 mL), dried over Na_2SO_4, filtered and concentrated in vacuo. The crude material was subsequently purified by column chromatography to afford the appropriate deaminated product.

General procedure of demethylation (for PT091–92, PT095–96, PT107–116, PT119, PT131, PT133–134, PT161, PT164): The methoxybenzene (0.627 mmol) was dissolved in dry CH_2Cl_2 (50 mL), and BBr_3 (0.94 mL, 2 M in CH_2Cl_2, 1.88 mmol) was added dropwise at −40 °C. The reaction was gradually warmed to RT and stirred for 3 h. When TLC showed completion, the reaction was cooled to −40 °C and quenched with MeOH. The solution was concentrated in vacuo to give the crude product. Purification by chromatography gave pure compounds.

4-(Benzyloxy)-3-methoxybenzaldehyde (1): Vanillin (10 g, 65.7 mmol), BnBr (12.4 g, 72.3 mmol) and KOH (4.1 g, 72.3 mmol) were dissolved in MeOH/H_2O (1:1, 150 mL) and heated at reflux for 2 h. After TLC showed completion, the reaction was diluted with H_2O (300 mL) and extracted with CH_2Cl_2 (2×100 mL). The combined organic layers were dried with $MgSO_4$, filtered and concentrated in vacuo to give the crude product. Purification by flash chromatography (EtOAc/petroleum ether, 8%) gave **1** as a white crystalline solid (14.5 g, 91%): ^{1}H NMR (400 MHz, $CDCl_3$): δ = 9.81 (s, 1H), 7.42–7.29 (m, 7H), 6.96 (d, J = 6.3 Hz, 1H), 5.22 (s, 2H), 3.92 ppm (s, 3H); ^{13}C NMR (100 MHz, $CDCl_3$): δ = 191.1, 153.8, 150.3, 136.2, 130.5, 128.9, 128.4, 127.4, 126.8, 112.6, 109.6, 71.09, 56.3 ppm; HRMS-ES+: m/z $[M+H]^+$ calcd for $C_{15}H_{15}O_3$: 243.1021, found: 243.1022.

1-(Benzyloxy)-4-(hex-1-en-1-yl)-2-methoxybenzene (2): nBuLi (2.45 mL, 4.9 mmol, 2 M in cyclohexane) was added dropwise to a solution of n-pentyl-triphenylphosphonium bromide (2 g, 4.9 mmol) in dry THF (100 mL) at −78 °C. After 30 min, a solution of **1** (1.0 g, 4.1 mmol) in dry THF (50 mL) was added dropwise. After an additional 30 min, the cooling bath was removed, and the reaction was stirred for another 1.5 h. When TLC showed completion, the reaction was quenched with 1 M aq HCl (5 mL) and diluted with H_2O (100 mL). The aqueous mixture was extracted with CH_2Cl_2 (3×25 mL), and the combined organic layers were dried over $MgSO_4$, filtered and concentrated in vacuo to give the crude product. Purification by flash chromatography (EtOAc/petroleum ether, 5%) gave **2** as a white crystalline solid (1.0 g, 82%): ^{1}H NMR (400 MHz, $CDCl_3$): δ = 7.27–7.43 (m, 5H), 6.91 (s, 1H), 6.79 (s, 1H), 6.29 (d, J = 11.7 Hz, 2H), 6.08 (td, J = 11.7, 5.1 Hz, 1H), 5.13 (s, 2H), 3.89 (s, 3H), 2.18 (dd, J = 5.1, 4.8 Hz, 2H), 1.46–1.29 (m, 4H), 0.91 ppm (t, J = 5.4 Hz, 3H); ^{13}C NMR (100 MHz, $CDCl_3$): δ = 150.0, 147.6, 137.5, 131.98, 129.7, 129.5, 28.7, 128.0, 127.5, 118.9, 114.5, 109.5, 71.4, 57.2, 32.9, 31.9, 22.5, 14.2 ppm; HRMS-ES+: m/z $[M+H]^+$ calcd for $C_{20}H_{24}O_2$: 297.1855, found: 297.1855.

4-Hexyl-2-methoxyphenol (3): Activated Pd/C (40 mg) was added to a solution of **2** (800 mg, 2.7 mmol) in EtOH (100 mL). The reaction was stirred under 1 atm of H_2 for 6 h and then filtered through Celite. The solvent was removed in vacuo to give the crude product. Flash chromatography (EtOAc/petroleum ether, 5%) gave **3** as a colorless oil (500 mg, 89%): ^{1}H NMR (400 MHz, $CDCl_3$): δ = 6.80 (d, J = 6.0 Hz, 1H), 6.65–6.63 (m, 2H), 5.42 (s, 1H), 3.85 (s, 3H), 2.50 (t, J = 5.7 Hz, 2H), 1.56–1.54 (m, 2H), 1.30–1.27 (m, 6H), 0.86 ppm (t, J = 5.1 Hz, 3H); ^{13}C NMR (100 MHz, $CDCl_3$): δ = 146.5, 143.7, 135.2, 121.1, 114.3, 111.1, 56.1, 35.9, 32.0, 32.0, 29.2, 22.8, 14.3 ppm; MS (ESI+, 70 eV): m/z (%): 209.0 (100) $[M+H]^+$; MS (ESI−, 70 eV): m/z (%): 207 (100) $[M-H]^-$.

4-Hexyl-2-methoxy-1-(2-(trifluoromethyl)phenoxy)benzene (4): 1-Iodo-2-(trifluoromethyl)benzene (2.0 g, 7.35 mmol), **3** (1.10 g, 7.35 mmol), Cs_2CO_3 (10.5 g, 32.3 mmol), $(CuOTf)_2$·PhH (185.0 mg, 0.37 mmol, 5.0 mol% Cu), and 1-naphthoic acid (5.56 g, 32.3 mmol) were dissolved in EtOAc (1 mL) and toluene (75 mL) in an oven-dried 150 mL two-necked round-bottomed flask. Molecular sieves (1.8 g, 4 Å) were added to the flask under a continuous stream of N_2, and then the flask was sealed with a septum and heated to 110 °C under N_2. After 24 h, upon cooling to RT, CH_2Cl_2 (50 mL) was added, and the mixture was filtered. The filtrate was washed with 5% aq NaOH (20 mL), and the aqueous layer was back-extracted with CH_2Cl_2 (2×25 mL). All organic layers including the original filtrate were combined and washed with brine (50 mL), dried over Mg_2SO_4, filtered and concentrated in vacuo to give the crude product. Purification by flash chromatography (EtOAc/hexane, 4%) gave **4** as a light yellow oil (1.94 g, 75%): MS (ESI+, 70 eV): m/z (%): 353.0 (100), 354.2 (21) $[M+H]^+$.

4-Hexyl-2-methoxy-1-(2-nitrophenoxy)benzene (5): A solution of **3** (800 mg, 3.8 mmol), 1-fluoro-2-nitrobenzene (536.2 mg, 3.8 mmol), and 18-crown-6 (50.2 mg, 0.19 mmol) in dry DMF (40 mL) was heated to 110 °C under N_2 and stirred for 3 h. The reaction was cooled to RT and partitioned between H_2O (200 mL) and CH_2Cl_2 (200 mL). The organic layer was separated, dried over $MgSO_4$, filtered and concentrated to give the crude product. Purification with flash chromatography (EtOAc/petroleum ether, 5%) gave **5** as a light yellow oil (826 mg, 66%): ^{1}H NMR (300 MHz, $CDCl_3$): δ = 7.94 (dd, J = 8.4, 1.5 Hz,1H), 7.40 (td, J = 7.5, 1.8 Hz, 1H), 7.08 (td, J = 7.5, 1.5 Hz, 1H), 6.99 (d, J = 7.8 Hz, 1H), 6.81 (dd, J = 8.4, 1.2 Hz, 1H), 6.80 (dd, J = 8.1, 1.8 Hz, 1H), 6.76 (d, J = 2.1 Hz, 1H), 3.77 (s, 3H), 2.61 (t, J = 7.8 Hz, 2H), 1.62 (m, 2H), 1.32 (m, 2H), 0.89 ppm (t, J = 6.9 Hz, 3H); ^{13}C NMR (100 MHz, $CDCl_3$): δ = 152.3, 151.3, 141.8, 141.3, 134.1, 125.8, 121.9, 121.2, 118.1, 113.6, 56.2, 36.1, 31.9, 31.8, 29.2, 22.8, 14.3 ppm; HRMS-ES+: m/z $[M+H]^+$ calcd for $C_{19}H_{23}NO_4$: 330.1705, found: 330.1703.

2-(Hexyl-2-methoxyphenoxy)aniline (6): Activated Pd/C (25 mg) was added to a solution of **5** (500 mg, 1.5 mmol) in EtOH (100 mL). The reaction was stirred under 1 atm of H_2 for 6 h and then filtered through Celite. The crude product was obtained by removal of the solvent in vacuo and used in the next step without further purification (413 mg, 91%): ^{1}H NMR (400 MHz, $CDCl_3$): δ = 6.88 (td, J = 5.7, 1.2 Hz, 1H), 6.78–6.75 (m, 3H), 6.72 (dd, J = 6.0 Hz, 1.2 Hz, 1H), 6.65 (dd, J = 5.1, 1.5 Hz, 1H), 6.62 (dd, J = 6.0, 1.2 Hz, 1H), 3.86 (s, 2H), 3.84 (s, 3H), 2.55 (t, J = 6.0 Hz, 2H), 1.59–1.56 (m, 2H), 1.32–1.28 (m, 6H), 0.87 ppm (t, J = 5.4 Hz, 3H); ^{13}C NMR (100 MHz, $CDCl_3$): δ = 150.5, 144.9, 143.5, 139.2, 138.1, 124,0, 120.8, 119.1, 118.7, 118.4, 116.4, 113.2, 56.9, 36.0, 31.9, 31.5, 29.2, 22.8, 14.3 ppm; HRMS-ES+: m/z $[M+H]^+$ calcd for $C_{19}H_{25}NO_2$: 300.1964, found: 300.1963.

1-(2-Chlorophenoxy)-4-hexyl-2-methoxybenzene (7): Compound **6** (300 mg, 1.0 mmol) and CuCl were reacted according to the gen-

eral procedure for diazotization to give **7** as a light yellow solid (188 mg, 59%). The crude material was used in the next step without purification. MS (ESI+, 70 eV): *m/z* (%): 319.2 (100) $[M+H]^+$.

1-(2-Bromophenoxy)-4-hexyl-2-methoxybenzene (8): Compound **6** (300 mg, 1.0 mmol) and CuBr were reacted according to the general procedure for diazotization, and purification by flash chromatography (EtOAc/petroleum ether, 5%) gave **8** as a yellow solid (233 mg, 64%): ^{1}H NMR (300 MHz, $CDCl_3$): $\delta=7.26$ (dd, $J=6.9$, 1.5 Hz, 1H), 7.18 (dd, $J=4.8$, 1.5 Hz, 1H), 6.96–6.64 (m, 5H), 3.82 (s, 3H), 2.60 (t, $J=7.5$ Hz, 2H), 1.65–1.60 (m, 2H), 1.33–1.22 (m, 6H), 0.90 ppm (t, $J=6.3$ Hz, 3H); MS (ESI+, 70 eV): *m/z* (%): 363.1 (100), 364.0 (21), 365.4 (100) $[M+H]^+$.

4-Hexyl-2-methoxy-1-(2-methoxy-4-nitrophenoxy)benzene (15): Compounds **3** (1.0 g, 4.8 mmol) and **11** (1.0 g, 5.8 mmol) were treated according to the general procedure for aromatic substitution to give **15** as a yellow solid (1.7 g, 98%): ^{1}H NMR (300 MHz, $CDCl_3$): $\delta=7.83$ (d, $J=2.4$ Hz, 1H), 7.74 (dd, $J=2.7$, 6.0 Hz, 1H), 6.98 (d, $J=7.8$ Hz, 1H), 6.80 (td, $J=7.8$, 1.8 Hz, 2H), 6.60 (d, $J=9.0$ Hz, 1H), 4.02 (s, 3H), 3.76 (s, 3H), 2.62 (t, $J=7.8$ Hz, 2H), 1.66–1.57 (m, 2H), 1.38–1.28 (m, 6H), 0.89 ppm (t, $J=6.9$ Hz, 3H); MS (ESI+, 70 eV): *m/z* (%): 360.3 (100), 361.1 (22) $[M+H]^+$.

1,3-Dichloro-2-(hexyl-2-methoxyphenoxy)-5-nitrobenzene (16): Compounds **3** (1.0 g, 4.8 mmol) and **12** (1.2 g, 5.8 mmol) were treated according to the general procedure for aromatic substitution to give **16** as a yellow solid (1.7 g, 88%): ^{1}H NMR (400 MHz): $\delta=8.24$ (s, 2H), 6.82 (s, 1H), 6.62 (d, $J=9.0$ Hz, 1H), 6.42 (d, $J=2.2$ Hz, 1H), 3.94 (s, 3H), 2.60 (t, $J=7.6$ Hz, 2H), 1.64–1.58 (m, 3H), 1.38–1.26 (m, 5H), 0.87 ppm (t, $J=6.7$ Hz, 3H).

2-Fluoro-1-(hexyl-2-methoxyphenoxy)-4-nitrobenzene (17): Compounds **3** (1.0 g, 4.8 mmol) and **13** (0.92 g, 5.8 mmol) were treated according to the general procedure for aromatic substitution to give **17** as a yellow solid (1.0 g, 60%): ^{1}H NMR (400 MHz,): $\delta=8.00$ (d, $J=10.2$ Hz,1H), 7.82 (d, $J=9.2$ Hz, 1H), 6.96 (d, $J=8.2$ Hz, 1H), 6.80–6.6.70 (m, 2H), 6.68 (t, $J=8.1$ Hz, 1H), 3.74 (s, 3H), 2.58 (t, $J=6.7$ Hz, 2H), 1.64–1.56 (m, 3H), 1.38–1.22 (m, 5H), 0.87 ppm (t, $J=6.6$ Hz, 3H).

1-Chloro-3-fluoro-2-(hexyl-2-methoxyphenoxy)-5-nitrobenzene (18): Compounds **3** (1.0 g, 4.8 mmol) and **14** (1.1 g, 5.8 mmol) were treated according to the general procedure for aromatic substitution to give **18** as a yellow solid (1.4 g, 77%): ^{1}HNMR (400 MHz, $CDCl_3$): $\delta=8.18$ (s, 1H), 7.91–7.90 (m, 1H), 6.80 (s, 1H), 6.72–6.64 (m, 2H), 3.82 (s, 3H), 2.58–2.52 (m, 2H), 1.62–1.54 (m, 3H), 1.38–1.24 (m, 5H), 0.94–0.84 ppm (m, 3H); HPLC: $t_R=8.4$ min (95% purity).

4-(Hexyl-2-methoxyphenoxy)-3-methoxyaniline (19): Compound **15** (800 mg, 83%) was treated according to the general procedure for reduction of nitrobenzene to give **19** as a yellow oil (609 mg, 1.8 mmol): MS (ESI+, 70 eV): *m/z* (%): 330.1 (100), 331.2 (22) $[M+H]^+$.

3-Chloro-5-fluoro-4-(hexyl-2-methoxyphenoxy) aniline (22): Compound **18** (800 mg, 2.1 mmol) was treated according to the general procedure for reduction of nitrobenzene to give **22** as a yellow solid (545 mg, 74%): ^{1}HNMR (400 MHz, $CDCl_3$): $\delta=6.80$ (s, 1H), 6.70 (s, 1H), 6.62–6.56 (m, 2H), 6.44 (d, $J=7.4$ Hz, 1H), 3.94 (s, 3H), 2.58 (t, $J=7.4$ Hz, 2H), 1.62–1.54 (m, 2H), 1.38–1.22 (m, 6H), 0.94–0.84 ppm (m, 3H); MS (ESI+, 70 eV): *m/z* (%): 352.3 (100), 353.1 (21), 354.4 (33) $[M+H]^+$; HPLC: $t_R=7.3$ min (96% purity).

4-Hexyl-2-methoxy-1-(2-methoxyphenoxy)benzene (23): Compound **19** (500 mg, 1.5 mmol) was treated according to the general procedure for deamination to give **23** as a yellow oil (406 mg, 85%): MS (ESI+, 70 eV): *m/z* (%): 315.2 (100), 316.1 (22) $[M+H]^+$.

1-(2,6-dichlorophenoxy)-3-hexyl-2-methoxybenzene (24): Compound **16** (800 mg, 2.0 mmol) was treated according to the general procedure for reduction of nitrobenzene to give **20** as a yellow solid (577 mg, 78%). Crude compound **20** (577 mg, 1.6 mmol) was further reacted according to the general procedure for deamination to give **24** as a yellow oil (486 mg, 86%): ^{1}H NMR (400 MHz, $CDCl_3$): $\delta=7.38$ (m, 2H), 7.16 (t, $J=8.5$ Hz, 1H), 6.82 (s, 1H), 6.58 (d, $J=8.1$ Hz, 1H), 6.32 (d, $J=7.6$ Hz, 1H), 3.80 (s, 3H), 2.56 (t, $J=7.5$ Hz, 2H), 1.62–1.54 (m, 3H), 1.38–1.24 (m, 5H), 0.94–0.86 ppm (m, 3H); HPLC: $t_R=11.8$ min (96% purity).

1-(2-Fluorophenoxy)-4-hexyl-2-methoxybenzene (25): Compound **17** (800 mg, 2.3 mmol) was treated according to the general procedure for reduction of nitrobenzene to give **21** as a yellow solid (599 mg, 82%). Crude compound **21** (599 mg, 1.9 mmol) was further reacted according to the general procedure for deamination to give **25** as a yellow oil (448 mg, 78%): ^{1}H NMR (400 MHz, $CDCl_3$): $\delta=7.17$–7.12 (m, 1H), 7.02–6.99 (m, 2H), 6.88–6.81 (m, 3H), 6.72–6.69 (dd, $J=8.2$, 2.2 Hz, 2H), 3.84 (s, 3H), 2.58 (t, $J=7.4$ Hz, 2H), 1.64–1.58 (m, 2H), 1.37–1.32 (m, 6H), 0.89 ppm (t, $J=6.6$ Hz, 3H); HRMS-ES+: *m/z* $[M+H]+$ calcd for $C_{19}H_{29}FO_2$: 303.1760, found: 300.1758; HPLC: $t_R=13.5$ min (98% purity).

1-Chloro-3-fluoro-2-(hexyl-2-methoxyphenoxy)benzene (26): Compound **22** (500 mg, 1.4 mmol) was treated according to the general procedure for deamination to give **26** as a yellow oil (407 mg, 85%): ^{1}H NMR (400 MHz, $CDCl_3$): $\delta=7.26$ (d, $J=7.6$ Hz, 1H), 7.18–7.04 (m, 2H), 6.82 (s, 1H), 6.62 (d, $J=8.2$ Hz, 1H), 6.42 (d, $J=7.9$ Hz, 1H), 3.94 (s, 3H), 2.59 (t, $J=6.9$ Hz, 2H), 1.68–1.54 (m, 3H), 1.42–1.24 (m, 6H), 1.89 ppm (t, $J=6.6$ Hz, 3H); MS (ESI+, 70 eV): *m/z* (%): 337.3 (100), 338.0 (21), 339.4 (33) $[M+H]^+$; HPLC: $t_R=11.3$ min (95.4% purity).

4-Hexyl-2-methoxy-1-(2-methyl-4-nitrophenoxy)benzene (27): Compound **3** (1.0 g, 4.8 mmol) and 1-fluoro-2-methyl-4-nitrobenzene (894 mg, 5.8 mmol) were reacted according to the general procedure for aromatic substitution to give **27** as a yellow solid (857 mg, 52%): MS (ESI+, 70 eV): *m/z* (%): 344.1 (100), 345.0 (22) $[M+H]^+$. The crude material was used in the next step without further purification.

1-(2,6-Dimethylphenoxy)-3-hexyl-2-methoxybenzene (28): 2-Bromo-1,3-dimethylbenzene (0.667 g, 3.6 mmol) and K_3PO_4 (1.0 g, 4.8 mmol) were added to a stirred solution of **3** (0.5 g, 2.403 mmol) in DMF (5 mL). The reaction mixture was degassed for 30 min, after which $Cu(bipy)_2BF_4$ (0.112 g, 0.24 mmol) was added, and the mixture was stirred at 120 °C for 48 h. After TLC showed that the reaction was complete, the solution was diluted with EtOAc (40 mL) and washed with water (2×40 mL). The organic layer was further washed with brine (60 mL), dried over Na_2SO_4, filtered and concentrated in vacuo. Purification by flash chromatography (EtOAc/hexane, 3%) gave **28** as a yellow solid (0.075 g, 10%): ^{1}H NMR (400 MHz, $CDCl_3$): $\delta=7.10$–7.02 (m, 2H), 6.80 (s, 1H), 6.54 (d, $J=7.4$ Hz, 1H), 6.20 (d, $J=8.0$ Hz, 2H), 3.98 (s, 3H), 2.54 (t, $J=7.5$ Hz, 2H), 2.18 (s, 3H), 1.64–1.48 (m, 6H), 1.38–1.24 (m, 5H), 0.89 ppm (t, $J=6.7$ Hz, 3H).

1-(2-Methyl-6-nitrophenoxy)-3-hexyl-2-methoxybenzene (29): Compound **3** (1.0 g, 4.8 mmol) and 2-fluoro-1-methyl-3-nitrobenzene (908 mg, 5.8 mmol) were reacted according to the general procedure for aromatic substitution to give **29** as a yellow solid (692 mg, 42%): ^{1}H NMR (400 MHz, $CDCl_3$): $\delta=7.80$ (d, $J=8.1$ Hz, 1H), 7.51 (d, $J=2.1$ Hz, 1H), 7.28–7.22 (m, 2H), 6.82 (s, 1H), 6.58 (d,

J=2.1 Hz, 1H), 6.38 (m, 1H), 3.88 (s, 3H), 2.56 (t, J=7.2 Hz, 2H), 2.22 (s, 3H), 1.62–1.54 (m, 3H), 1.38–1.22 (m, 5H), 0.89 ppm (t, J=6.7 Hz, 3H); MS (ESI+, 70 eV): m/z (%): 366.1 (100) $[M+Na]^+$; HPLC: t_R=12.3 min (99% purity).

2-(Hexyl-2-methoxyphenoxy)-3-methylbenzenamine (30): Compound **29** (500 mg, 1.5 mmol) was treated according to the general procedure for reduction of nitrobenzene to give **30** as a dark yellow solid (187 mg, 41%): ^{1}H NMR (400 MHz, $CDCl_3$): δ=6.99–6.94 (t, J=8.4 Hz, 1H), 6.78 (d, J=7.6 Hz, 2H), 6.64 (m, 1H), 6.59 (m, 1H), 6.42 (m, 1H), 3.89 (s, 3H), 2.56 (t, J=7.5 Hz, 2H), 2.18 (s, 3H), 1.62–1.54 (m, 2H), 1.42–1.24 (m, 5H), 0.89 ppm (t, J=6.5 Hz, 3H); MS (ESI+, 70 eV): m/z (%): 314.0 (100), 315.3 (22) $[M+H]^+$; HPLC: t_R=11.7 min (99% purity).

2-(Hexyl-2-methoxyphenoxy)-3-fluorobenzonitrile (31): Compound **3** (1.0 g, 4.8 mmol) and 2-bromo-3-fluorobenzonitrile (1.2 g, 5.8 mmol) were reacted according to the general procedure for aromatic substitution to give **31** as a yellow solid (629 mg, 40%): ^{1}H NMR (400 MHz, $CDCl_3$): δ=7.38–7.22 (m, 3H), 6.98 (d, J=8.2 Hz, 1H), 6.82–6.78 (m, 2H), 6.72 (d, J=7.8 Hz, 1H), 3.78 (s, 3H), 2.63 (t, J=7.4 Hz, 2H), 1.72–1.64 (m, 3H), 1.42–1.24 (m, 6H), 0.92 ppm (t, J=6.8 Hz, 3H); HPLC: t_R=11.0 min (95% purity).

2-(Hexyl-2-methoxyphenoxy)-3-fluorobenzamidine (32): Li(TMS)$_2$ (0.18 g, 1.18 mmol) was added to a stirred solution of **31** (0.2 g, 0.61 mmol) in THF (2 mL) at 0 °C, and the reaction was stirred at RT for 3 h. After the reaction was shown to be complete by TLC, the mixture was diluted with H_2O (15 mL) and extracted with CH_2Cl_2 (2×30 mL). The combined organic layers were washed with brine (15 mL), dried over Na_2SO_4, filtered and concentrated in vacuo. Purification by flash chromatography (MeOH/CH_2Cl_2, 1%) gave **32** as a yellow solid (0.096 g, 46%): ^{1}H NMR (400 MHz, $CDCl_3$): δ=8.96 (br s, 1H), 7.98 (s, 2H), 7.42 (d, J=8.0 Hz, 1H), 7.12–7.03 (m, 2H), 6.90–6.81 (m, 2H), 6.74 (d, J=7.6 Hz, 1H), 3.80 (s, 3H), 2.60 (t, J=7.2 Hz, 2H), 1.66–1.60 (m, 2H), 1.42–1.38 (m, 6H), 0.98–0.92 ppm (m, 3H); MS (ESI+, 70 eV): m/z (%): 345.0 (100) $[M+H]^+$; HPLC: t_R=9.4 min (64% purity).

3-(Hexyl-2-methoxyphenoxy)-2-nitropyridine (34): Compound **3** (0.5 g, 2.4 mmol) was added to 5% aq NaOH (7.68 g, 9.61 mmol) and stirred for 10 min. The solution was concentrated in vacuo, and the residue was redissolved in CH_3CN (5 mL). The solution was treated with 3-bromo-2-nitropyridine (0.455 g, 2.88 mmol), and the reaction mixture was heated at reflux for 2 h. After the reaction was shown to be complete by TLC, the mixture was filtered, and the filtrate was partitioned between H_2O (15 mL) and CH_3CN (50 mL). The organic layer was separated, dried over Na_2SO_4, filtered and concentrated in vacuo. Purification by flash chromatography (EtOAc/hexane, 10%) gave **34** as a yellow solid (0.13 g, 16%): ^{1}H NMR (400 MHz, $CDCl_3$): δ=8.37 (d, J=8.1 Hz, 1H), 8.31 (d, J=5.0 Hz, 1H), 7.10–7.09 (m, 2H), 6.82 (d, J=6.0 Hz, 2H), 3.71 (s, 3H), 2.62 (t, J=8.0 Hz, 2H), 1.64–1.44 (m, 2H), 1.35–1.32 (m, 6H), 0.90 ppm (t, J=6.5 Hz, 3H); ^{13}C NMR (100 MHz, $CDCl_3$): δ=156.1, 151.8, 150.9, 141.8, 139.3, 135.2, 133.9, 122.4, 120.7, 117.7, 113.1, 55.9, 35.9, 31.6, 31.2, 29.0, 22.5, 14.0 ppm; HRMS-ES+: m/z $[M+H]^+$ calcd for $C_{18}H_{22}N_2O_4$: 331.1658, found: 331.1652; HPLC: t_R=10.1 min (76% purity).

3-(Hexyl-2-methoxyphenoxy)pyridin-2-amine (35): Fe powder (81 mg, 3.1 mmol) was added to a stirred solution of **34** (128 mg, 0.38 mmol) in AcOH/H_2O (4:1, 5 mL), and the mixture was then heated at reflux for 30 min. After the reaction was shown to be complete by TLC, the mixture was filtered, and the filtrated was first diluted with water and then extracted with CH_2Cl_2 (40 mL). The organic layer was separated, washed with brine (50 mL), dried over anhydrous Na_2SO_4, filtered and concentrated in vacuo to give **35** (92 mg, 77%): MS (ESI+, 70 eV): m/z (%): 301.2 (100), 302.0 (20) $[M+H]^+$. The crude material was used in the next step without further purification.

3-(Hexyl-2-methoxyphenoxy)-4-nitropyridine 1-oxide (36): Compound **3** (0.5 g, 2.4 mmol) was added to a solution of NaOH (0.385 g, 9.6 mmol) in H_2O (1 mL), and the mixture was stirred for 5 min at RT. The water was removed in vacuo to afford a white solid, which was taken up in CH_3CN (7 mL), and the resultant solution was treated with 3-bromo-4-nitropyridine 1-oxide (0.63 g, 2.8 mmol). The mixture was heated at reflux for 2 h and, after the reaction was shown to be complete by TLC, the reaction mixture was filtered, and the filtrate was concentrated in vacuo. Purification by flash chromatography (EtOAc/hexane, 50%) gave **36** as a dark yellow solid (0.5 g, 60%): ^{1}H NMR (400 MHz, $CDCl_3$): δ=7.86 (d, J=2.2 Hz, 1H), 7.84 (d, J=8.0 Hz, 1H), 7.74 (s, 1H), 7.04 (d, J=7.8 Hz, 1H), 6.82 (m, 2H), 3.78 (s, 3H), 2.60 (t, J=7.6 Hz, 2H), 1.64–1.58 (m, 3H), 1.38–1.26 (m, 5H), 0.89 ppm (t, J=6.7 Hz, 3H); MS (ESI+, 70 eV): m/z (%): 347.2 (100), 348.1 (20) $[M+H]^+$.

3-(Hexyl-2-methoxyphenoxy)pyridin-4-amine (37): A stirred solution of **36** (0.5 g, 1.4 mmol) in AcOH/H_2O (8:2, 100 mL) was heated to 80 °C, and Fe powder (4.0 g, 72 mmol) was added portionwise at 80 °C. The mixture was stirred at the same temperature for 2 h. After the reaction was shown to be complete by TLC, the reaction mixture was cooled to RT, quenched with water and extracted with CH_2Cl_2 (2×20 mL). The combined organic layers were washed with brine (15 mL), dried over Na_2SO_4, filtered and concentrated in vacuo. Purification by flash chromatography (MeOH/CH_2Cl_2, 5%) gave **37** as a dark yellow oil (0.25 g, 57%): HRMS-ES+: m/z $[M+H]^+$ calcd for $C_{18}H_{24}N_2O_2$: 301.1916, found: 301.1906.

3-(Hexyl-2-methoxyphenoxy)isonicotinonitrile (38): Compound **3** (1.0 g, 4.8 mmol) and 3-chloroisonicotinonitrile (0.8 g, 5.8 mmol) were reacted according to the general procedure for aromatic substitution to give **38** as a dark yellow oil (1.0 g, 69%): ^{1}H NMR (400 MHz, $CDCl_3$): δ=8.38 (d, J=1.5 Hz, 1H), 8.14 (s, 1H), 7.46 (d, J=8.0 Hz, 1H), 7.12 (d, J=7.8 Hz, 1H), 6.82 (d, J=7.5 Hz, 2H), 3.78 (s, 3H), 2.62 (t, J=7.4 Hz, 2H), 1.66–1.62 (m, 2H), 1.42–1.34 (m, 6H), 0.91 ppm (t, J=6.6 Hz, 3H); HPLC: t_R=10.5 min (98% purity).

3-(Hexyl-2-methoxyphenoxy)isonicotinic acid (39): KOH pellets (0.025 g, 0.45 mmol) were added to a stirred solution of **38** (0.07 g, 0.15 mmol) in MeOH (2 mL) at >RT. The reaction mixture was then heated at reflux for 2 h. After the reaction was shown to be complete by TLC, the reaction mixture was neutralized with 1 N aq HCl (pH 1–2) and extracted with CH_2Cl_2 (2×20 mL). The combined organic layers were washed with H_2O (10 mL), dried over Na_2SO_4, filtered and concentrated in vacuo. Purification by HPLC gave **39** as a dark yellow oil (61 mg, 82%): ^{1}H NMR (400 MHz, [D_6]DMSO): δ=13.56 (s, 1H), 8.38 (d, J=2.1 Hz, 1H), 7.98 (s, 1H), 7.62 (d, J=2.2 Hz, 1H), 7.00 (s, 1H), 6.94 (d, J=8.0 Hz, 1H), 6.78 (d, J=7.8 Hz, 1H), 3.78 (s, 3H), 2.60 (t, J=7.4 Hz, 2H), 1.60 (t, J=6.8 Hz, 2H), 1.38–1.24 (m, 6H), 0.89 ppm (t, 3H).

Ethyl 2-(hexyl-2-methoxyphenoxy) acetate (40): A solution of **3** (2 g, 9.6 mmol) in EtOH (5 mL) was added to a solution of NaOEt (4.6 mL, 14.4 mmol) in EtOH (15 mL) at RT. Ethyl bromoacetate (1.6 mL, 14.4 mmol) was added dropwise, and the reaction mixture was heated at reflux for 16 h. After the reaction was shown to be complete by TLC, the solvent was removed in vacuo, H_2O was added, and the mixture was extracted with EtOAc (2×50 mL). The combined organic layers were washed with brine (50 mL), dried over Na_2SO_4, filtered and concentrated in vacuo. Purification by flash chromatography (EtOAc/hexane, 10%) gave **40** as a yellow

solid (0.98 g, 35%): ^{1}H NMR (400 MHz, $CDCl_3$): δ=6.78 (d, J=8.2 Hz, 1H), 6.72 (s, 1H), 6.64 (d, J=7.8 Hz, 1H), 4.70 (s, 2H), 4.26 (t, J=7.4 Hz, 2H), 3.82 (s, 3H), 2.57 (t, J=7.2 Hz, 3H), 1.62–1.54 (m, 4H), 1.38–1.24 ppm (m, 6H); MS (ESI+, 70 eV): m/z (%): 295.4 (100), 296.1 (19) $[M+H]^+$; HPLC: t_R=9.2 min (97% purity).

5-(Hexyl-2-methoxyphenoxy) pyrimidin-4-ol (41): Compound **40** (1 g, 3.4 mmol) and ethyl formate (2.5 g, 34 mmol) were added to a stirred solution of NaH (0.146 g, 6.1 mmol) in THF (10 mL) at RT. The mixture was then heated at 65 °C for 4 h. After the reaction was shown to be complete by TLC, the solvent was removed in vacuo, and the crude material was redissolved in MeOH/EtOH (1:1, 12 mL). Formamidine acetate (0.353 g, 3.4 mmol) was added, and the reaction was stirred at 80 °C for 4 h. After the reaction was shown to be complete by TLC, the solvent was removed in vacuo, and the crude was purified by flash chromatography (MeOH/CH_2Cl_2, 8%) to give **41** as a yellow solid (0.47 g, 47%): ^{1}H NMR (400 MHz, $CDCl_3$): δ=7.88 (s, 1H), 7.38 (s, 1H), 6.99 (d, J=8.0 Hz, 1H), 6.82–6.78 (m, 2H), 3.82 (s, 3H), 2.60 (t, J=7.2 Hz, 2H), 1.68–1.48 (m, 4H), 1.38–1.22 (m, 4H), 0.89 ppm (t, J=6.8 Hz, 3H); HRMS-ES+: m/z $[M+H]^+$ calcd for $C_{17}H_{22}N_2O_3$: 303.1709, found: 303.1708; HPLC: t_R=7.3 min (99% purity).

4-Chloro-5-(hexyl-2-methoxyphenoxy) pyrimidine (42): $POCl_3$ (0.3 mL) was added dropwise to a stirred solution of **41** (25 mg, 0.08 mmol) in $CHCl_3$ (5 mL). The reaction was heated to 70 °C and stirred for 3 h. After the reaction was shown to be complete by TLC, the solvent was removed in vacuo, and the residue was dissolved in CH_2Cl_2 (20 mL). The organic phase was washed with water (2×20 mL) and brine (20 mL), dried over Na_2SO_4, filtered and concentrated in vacuo. Purification by flash chromatography (MeOH/CH_2Cl_2, 5%) gave **42** as a dark yellow solid (12 mg, 46%): ^{1}H NMR (400 MHz, $CDCl_3$): δ=7.93 (s, 1H), 7.38 (s, 1H), 6.96 (d, J=7.8 Hz, 1H), 6.88–6.81 (m, 2H), 3.80 (s, 3H), 2.58–2.54 (t, J=7.2 Hz, 2H), 1.62–1.54 (m, 2H), 1.38–1.24 (m, 6H), 0.98–0.92 ppm (m, 3H).

5-(Hexyl-2-methoxyphenoxy)pyrimidin-4-amine (43): NH_4OH (1.5 mL, 27 mmol) was added dropwise to a stirred solution of **42** (55 mg, 0.17 mmol) in CH_2Cl_2 (10 mL) at RT, and then the mixture was heated at 130 °C for 18 h. After the reaction was shown to be complete by TLC, the solvent was removed in vacuo, and the crude product purified by column chromatography (MeOH/CH_2Cl_2, 8%) to give **43** as a dark yellow oil (45 mg, 87%): ^{1}H NMR (400 MHz, $CDCl_3$): δ=8.30 (s, 1H), 7.70 (s, 1H), 6.90 (d, J=8.2 Hz, 1H), 6.80 (s, 1H), 6.75 (d, J=7.9 Hz, 1H), 5.20 (br s, 2H), 4.80 (s, 3H), 2.64 (t, J=7.4 Hz, 2H), 1.70–1.50 (m, 2H), 1.40–1.20 (m, 6H), 0.85 ppm (t, J=6.7 Hz, 3H); HRMS-ES+: m/z $[M+H]^+$ calcd for $C_{17}H_{23}N_3O_2$: 302.1869, found: 302.1868; HPLC: t_R=6.9 min (96% purity).

2-(2-Chlorophenoxy)-5-hexylphenol (PT091): Compound **7** (300 mg, 0.94 mmol) was treated according to the general demethylation procedure. Purification by flash chromatography (EtOAc/petroleum ether, 5%) gave **PT091** as a light yellow oil (255 mg, 89%): ^{1}H NMR (400 MHz, $CDCl_3$): δ=7.45 (dd, J=7.9, 1.6 Hz, 1H), 7.20 (td, J=8.0, 1.0 Hz, 1H), 7.07 (td, J=7.9, 1.5 Hz, 1H), 6.96 (dd, J=8.0, 1.5 Hz, 1H), 6.88 (d, J=2.0 Hz, 1H), 6.71 (d, J=8.2 Hz, 1H), 6.64 (dd, J=8.2, 2.0 Hz, 1H), 5.50 (s, 1H), 2.55 (t, J=7.9 Hz, 2H), 1.61–1.58 (m, 2H), 1.37–1.26 (m, 6H), 0.89 ppm (t, J=9.0 Hz, 1H); ^{13}C NMR (100 MHz, $CDCl_3$): δ=152.5, 147.7, 141.1, 140.3, 130.8, 128.0, 124.9, 124.6, 120.5, 119.2, 118.0, 116.3, 35.5, 31.7, 31.4, 28.9, 22.6, 14.1 ppm; HRMS-ES+: m/z $[M+NH_4]^+$ calcd for $C_{18}H_{21}ClO_2$: 322.1230, found: 322.1572.

2-(2-Bromophenoxy)-5-hexylphenol (PT092): Compound **8** (300 mg, 0.83 mmol) was treated according to the general demethylation procedure. Purification by flash chromatography (EtOAc/petroleum ether, 5%) gave **PT092** as a light yellow oil (236 mg, 82%): ^{1}H NMR (400 MHz, $CDCl_3$): δ=7.58 (dd, J=7.8, 1.6 Hz, 1H), 7.36 (td, J=8.0, 1.2 Hz, 1H), 7.02 (td, J=7.8, 1.6 Hz, 1H), 6.93 (dd, J=8.0, 1.2 Hz, 1H), 6.80 (d, J=2.0 Hz, 1H), 6.75 (d, J=8.2 Hz, 1H), 6.68 (dd, J=8.2, 2.0 Hz, 1H), 5.32 (s, 1H), 2.60 (t, J=8.0 Hz, 2H), 1.62–1.58 (m, 2H), 1.32–1.21 (m, 6H), 0.80 ppm (t, J=9.0 Hz, 1H); ^{13}C NMR (100 MHz, $CDCl_3$): δ=154.5, 152.1, 143.2, 138.7, 131.9, 126.3, 125.1, 124.6, 123.5, 117.1, 113.0, 110.4, 35.9, 31.8, 31.1, 28.8, 22.5, 14.2 ppm; HRMS-ES+: m/z $[M+NH_4]^+$ calcd for $C_{18}H_{21}BrO_2$: 348.0725, found: 348.0732.

5-Hexyl-2-(2-(trifluoromethyl)phenoxy)phenol (PT095): Compound **4** (1.0 g, 2.8 mmol) was treated according to the general demethylation procedure. Purification by flash chromatography (EtOAc/petroleum ether, 5%) gave **PT095** as a light yellow oil (844 mg, 88%): ^{1}H NMR (300 MHz, $CDCl_3$): δ=7.67 (dd, J=7.8, 1.5 Hz, 1H), 7.44 (td, J=7.8, 1.2 Hz, 1H), 7.16 (tt, J=8.1, 0.9 Hz, 1H), 6.93 (d, J=8.4 Hz, 1H), 6.90 (d, J=2.1 Hz, 1H), 6.86 (d, J=8.4 Hz, 1H), 6.69 (dd, J=8.1, 1.8 Hz, 1H), 5.43 (s, 1H), 2.57 (t, J=7.8 Hz, 2H), 1.64–1.56 (m, 2H), 1.37–1.28 (m, 6H), 0.90 ppm (m, 3H); HRMS-ES+: m/z $[M+Na]^+$ calcd for $C_{19}H_{21}F_3O_2$: 361.1391, found: 361.1396.

5-Hexyl-2-(2-iodophenoxy)phenol (PT096): Compound **6** (300 mg, 1.0 mmol) and CuI (286 mg, 1.5 mmol) were reacted according to the general procedure for diazotization to give **9** (269 mg, 68%). Crude **9** was then reacted further according to the general demethylation procedure, and purification of the product by flash chromatography (EtOAc/petroleum ether, 5%) gave **PT096** as a light yellow oil (334 mg, 84%): HRMS-ES+: m/z $[M+Na]^+$ calcd for $C_{18}H_{21}IO_2$: 419.0484, found: 419.0479.

5-Hexyl-2-(2-methyl-4-nitrophenoxy)phenol (PT107): Compound **27** (200 mg, 0.59 mmol) was treated according to the general demethylation procedure, and purification of the product by flash chromatography (EtOAc/hexane, 15%) gave **PT107** as a yellow solid (169 mg, 88%): ^{1}H NMR (300 MHz, $CDCl_3$): δ=8.10 (dd, J=0.6, 1.8 Hz, 1H), 7.94 (ddd, J=0.6, 3.0, 9.3 Hz, 1H), 6.91 (d, J=2.1 Hz, 1H), 6.75 (m, 2H), 6.71 (d, J=1.8 Hz, 1H), 5.41 (s, 1H), 2.58 (t, J=7.8 Hz, 2H), 2.44 (s, 3H), 1.61 (m, 2H), 1.32 (m, 6H), 0.89 ppm (t, J=6.9 Hz, 3H); HRMS-ES+: m/z $[M+Na]^+$ calcd for $C_{19}H_{23}NO_4$: 352.1525, found: 352.1528.

2-(2,6-Dimethylphenoxy)-5-hexylphenol (PT108): Compound **28** (200 mg, 0.64 mmol) was treated according to the general demethylation procedure, and purification of the product by flash chromatography (EtOAc/hexane, 15%) gave **PT108** as a dark yellow oil (153 mg, 80%): ^{1}H NMR (400 MHz, $CDCl_3$): δ=7.11–7.07 (m, 3H), 6,86 (s, 1H), 6.48 (d, J=8.2 Hz, 1H), 6.20 (d, J=7.8 Hz, 1H), 5.78 (br s, 1H), 2.51 (t, J=7.8 Hz, 2H), 2.14 (s, 6H), 1.58 (t, J=6.9 Hz, 2H), 1.30–1.26 (m, 6H), 0.88–0.86 ppm (t, 3H); HRMS-ES+: m/z $[M+Na]^+$ calcd for $C_{20}H_{26}O_2$: 321.1831, found: 321.1832; HPLC: t_R=12.6 min (94% purity).

2-(2,6-Dichlorophenoxy)-5-hexylphenol (PT109): Compound **24** (300 mg, 0.85 mmol) was treated according to the general demethylation procedure, and purification of the product by flash chromatography (EtOAc/hexane, 10%) gave **PT109** as a dark yellow oil (274 mg, 95%): ^{1}H NMR (400 MHz, $CDCl_3$): δ=7.40 (d, J=9.0 Hz, 2H), 7.26–7.20 (t, J=8.5 Hz, 1H), 6.87 (d, J=2.2 Hz, 1H), 6.54–6.52 (dd, J=8.8, 1.8 Hz, 1H), 6.33 (d, J=8.2 Hz, 2H), 5.72 (br s, 1H), 2.51 (t, J=7.5 Hz, 2H), 1.59–1.55 (m, 2H), 1.36–1.24 (m, 6H), 0.87 ppm (t, J=6.6 Hz, 3H); HRMS-ES+: m/z $[M+Na]^+$ calcd for $C_{18}H_{20}Cl_2O_2$: 361.0738, found: 361.0746; HPLC: t_R=10.5 min (99% purity).

2-(2-Amino-6-methylphenoxy)-5-hexylphenol (PT110): Compound **30** (200 mg, 0.64 mmol) was treated according to the general demethylation procedure, and purification of the product by flash chromatography (EtOAc/hexane, 10%) gave **PT110** as a dark yellow oil (122 mg, 64%): ^{1}H NMR (400 MHz, [D$_6$]DMSO): δ = 9.11 (s, 1H), 6.83 (t, J = 8.7 Hz, 1H), 6.69 (s, 1H), 6.62 (d, J = 8.2 Hz, 1H), 6.46–6.41 (m, 2H), 6.22 (d, J = 7.6 Hz, 1H), 4.71 (s, 1H), 2.42 (t, J = 7.8 Hz, 2H), 1.98 (s, 3H), 1.54–1.48 (m, 2H), 1.34–1.22 (m, 6H), 0.94–0.82 ppm (m, 3H); HRMS-ES+: m/z $[M+H]^+$ calcd for $C_{19}H_{25}NO_2$: 300.1964, found: 300.1959; HPLC: t_R = 10.5 min (99% purity).

3-Fluoro-2-(4-hexyl-2-hydroxyphenoxy)benzonitrile (PT111): Compound **31** (200 mg, 0.61 mmol) was treated according to the general demethylation procedure, and purification of the product by flash chromatography (EtOAc/hexane, 10%) gave **PT111** as a yellow solid (103 mg, 54%): ^{1}H NMR (400 MHz, CDCl$_3$): δ = 7.35–7.34 (d, J = 2.2 Hz, 1H), 7.27–7.23 (m, 1H), 7.00 (d, J = 9.2 Hz, 1H), 6.83 (d, J = 1.8 Hz, 1H), 6.70 (d, J = 8.5 Hz, 1H), 6.63–6.62 (d, J = 8.5, Hz, 2H), 5.24 (br s, 1H), 2.49 (t, J = 7.4 Hz, 2H), 1.53–1.51 (m, 2H), 1.26–1.18 (m, 6H), 0.82–0.80 ppm (m, 3H); HPLC: t_R = 10.4 min (99% purity).

2-((4-Aminopyridin-3-yl)oxy)-5-hexylphenol (PT112): Compound **37** (300 mg, 1.0 mmol) was treated according to the general demethylation procedure, and purification of the product by flash chromatography (EtOAc/hexane, 10%) gave **PT112** as a brown solid (97 mg, 34%): ^{1}H NMR (400 MHz, [D$_6$]DMSO): δ = 9.37 (s, 1H), 7.80 (d, J = 1.8 Hz, 1H), 7.60 (s, 1H), 6.75 (d, J = 8.1 Hz, 1H), 6.73 (d, J = 2.2 Hz, 1H), 6.64 (d, J = 8.2 Hz, 1H), 6.58–6.56 (dd, J = 8.1, 2.1 Hz,1H), 5.90 (s, 2H), 2.47 (t, J = 7.8 Hz, 2H), 1.54–1.50 (m, 2H), 1.27–1.22 (m, 6H), 0.86 ppm (t, J = 6.7 Hz, 3H); HRMS-ES+: m/z $[M+H]^+$ calcd for $C_{17}H_{22}N_2O_2$: 287.1760, found: 287.1761; HPLC: t_R = 7.4 min (98% purity).

2-(2-Fluorophenoxy)-5-hexylphenol (PT113): Compound **25** (300 mg, 1.0 mmol) was treated according to the general demethylation procedure, and purification of the product by flash chromatography (EtOAc/hexane, 10%) gave **PT113** as a yellow oil (126 mg, 44%): ^{1}H NMR (400 MHz, CDCl$_3$): δ = 7.20–7.18 (m, 1H), 7.17–6.99 (m, 3H), 6.87 (d, J = 7.8 Hz, 1H), 6.72 (d, J = 2.4 Hz, 1H), 6.64–6.62 (dd, J = 7.8, 2.2 Hz, 1H), 5. 65 (s 1H), 2.54 (t, J = 7.5 Hz, 2H), 1.58 (t, J = 7.8 Hz, 2H), 1.35–1.25 (m, 6H), 0.88 ppm (t, J = 6.5 Hz, 3H); HRMS-ES+: m/z $[M+Na]^+$ calcd for $C_{18}H_{21}FO_2$: 311.1423, found: 311.1433; HPLC: t_R = 12.2 min (98% purity).

5-Hexyl-2-(2-hydroxyphenoxy)phenol (PT114): Compound **23** (300 mg, 1.0 mmol) was treated according to the general demethylation procedure, and purification of the product by flash chromatography (EtOAc/hexane, 20%) gave **PT114** as a yellow oil (152 mmol, 53%): ^{1}H NMR (300 MHz, CDCl$_3$): δ = 7.03–7.00 (m, 2H), 6.87 (d, J = 2.4 Hz, 1H), 6.82–6.80 (m, 2H), 6.76 (d, J = 8.4 Hz, 1H), 6.65 (dd, J = 2.4, 8.4 Hz, 1H), 6.00 (s, 2H), 2.54 (t, J = 7.8 Hz, 2H), 2.03 (s, 2H), 1.59–1.57 (m, 2H), 1.36–1.27 (m, 6H), 0.91 ppm (t, J = 6.6 Hz, 3H); HRMS-ES+: m/z $[M+Na]^+$ calcd for $C_{18}H_{22}O_3$: 309.1467, found: 309.1466.

3-(4-Hexyl-2-hydroxyphenoxy)isonicotinonitrile (PT115): Compound **38** (200 mg, 0.64 mmol) was treated according to the general demethylation procedure, and purification of the product by flash chromatography (EtOAc/hexane, 10%) gave **PT115** as a dark yellow oil (80 mg, 42%): ^{1}H NMR (400 MHz, CDCl$_3$): δ = 8.46 (d, J = 1.8 Hz, 1H), 8.34 (s, 1H), 7.56 (d, J = 2.1 Hz, 1H), 6.92 (d, J = 8.2 Hz, 1H), 6.78 (d, J = 8.0 Hz, 1H), 5.38 (s, 1H), 2.62–2.58 (m, 2H), 1.64–1.54 (m, 3H), 1.38–1.24 (m, 5H), 0.94–0.84 ppm (m, 3H); HRMS-ES+: m/z $[M+H]^+$ calcd for $C_{18}H_{20}N_2O_2$: 297.1603, found: 297.1599; HPLC: t_R = 9.8 min (96% purity).

3-(4-Hexyl-2-hydroxyphenoxy)isonicotinic acid (PT116): Compound **39** (200 mg, 0.61 mmol) was treated according to the general demethylation procedure, and purification of the product by flash chromatography (EtOAc/hexane, 10%) gave **PT116** as a dark yellow oil (144 mg, 75%): ^{1}H NMR (400 MHz, [D$_6$]DMSO): δ = 8.32 (d, J = 1.8 Hz, 1H), 8.02 (s, 1H), 7.58 (d, J = 2.2 Hz, 1H), 6.98 (d, J = 9.1 Hz, 1H), 6.78 (s, 1H), 6.62 (d, J = 8.8 Hz, 1H), 2.58–2.44 (m, 2H), 1.58–1.46 (m, 2H), 1.36–1.24 (m, 6H), 0.94–0.84 ppm (m, 3H); HRMS-ES+: m/z $[M+H]^+$ calcd for $C_{18}H_{21}NO_4$: 316.1549, found: 316.1541; HPLC: t_R = 7.7 min (93% purity).

2-(4-Hexyl-2-hydroxyphenoxy)benzonitrile (PT119): Compound **6** (300 mg, 1.0 mmol) and CuCN were reacted according to general procedure for diazotization to give **10** (216 mg, 73%). Crude product **10** was then further treated according to the general demethylation procedure, and purification with flash chromatography (EtOAc/petroleum ether, 5%) gave **PT119** as a white solid (244 mg, 86%): ^{1}H NMR (300 MHz, CDCl$_3$): δ = 7.64 (br d, J = 7.8 Hz, 1H), 7.46 (br t, J = 8.1 Hz, 1H), 7.12 (br t, J = 7.5 Hz, 1H), 6.90–6.83 (m, 3H), 6.72 (br d, J = 8.1 Hz, 1H), 5.55 (s, 1H), 2.57 (t, J = 7.5 Hz, 2H), 1.60 (br t, J = 6.6 Hz, 2H), 1.36–1.24 (m, 6H), 0.88 ppm (t, J = 6.6 Hz, 3H); HRMS-ES+: m/z $[M+H]^+$ calcd for $C_{19}H_{21}NO_2$: 296.1651, found: 296.1647.

3-Fluoro-2-(4-hexyl-2-hydroxyphenoxy)benzimidamide (PT131): Compound **32** (200 mg, 0.58 mmol) was treated according to the general demethylation procedure, and purification with flash chromatography (EtOAc/petroleum ether, 5%) gave **PT131** as a dark yellow solid (119 mg, 62%): ^{1}H NMR (400 MHz, CDCl$_3$): δ = 9.12 (br s, 1H), 8.30 (s, 2H), 7.58–7.52 (m, 1H), 7.32–7.18 (m, 2H), 6.88 (s, 1H), 6.76 (d, J = 8.1 Hz, 1H), 6.58 (d, J = 7.8 Hz, 1H), 2.44 (t, J = 7.8 Hz, 2H), 1.56–1.44 (m, 2H), 1.36–1.22 (m, 6H), 0.86 ppm (t, J = 6.7 Hz, 3H); HRMS-ES+: m/z $[M+H]^+$ calcd for $C_{19}H_{23}FN_2O_2$: 331.1822, found: 331.1825; HPLC: t_R = 8.9 min (91% purity).

2-(2-Chloro-6-fluorophenoxy)-5-hexylphenol (PT133): Compound **26** (300 mg, 0.89 mmol) was treated according to the general demethylation procedure, and purification with flash chromatography (EtOAc/petroleum ether, 5%) gave **PT133** (242 mg, 84%): ^{1}H NMR (400 MHz, CDCl$_3$): δ = 7.28 (d, J = 8.1 Hz, 1H), 7.18–7.10 (m, 2H), 6.84 (s, 1H), 6.56 (d, J = 7.8 Hz, 1H), 6.42 (d, J = 8.0 Hz, 1H), 5.68 (s, 1H), 2.54 (t, J = 7.5 Hz, 2H), 1.62–1.54 (m, 2H), 1.36–1.24 (m, 6H), 0.89 ppm (t, J = 6.6 Hz, 3H); HRMS-ES+: m/z $[M+Na]^+$ calcd for $C_{18}H_{20}ClFO_2$: 345.1034, found: 345.1032; HPLC: t_R = 10.0 min (95% purity).

2-((4-Aminopyrimidin-5-yl)oxy)-5-hexylphenol (PT134): Compound **43** (200 mg, 0.66 mmol) was treated according to the general demethylation procedure, and purification with flash chromatography (EtOAc/petroleum ether, 5%) gave **PT134** as a dark yellow oil (130 mg, 68%): ^{1}H NMR (400 MHz, CDCl$_3$): δ = 8.18 (s, 1H), 7.38 (s, 1H), 6.98 (d, J = 8.1 Hz, 1H), 6.82 (s, 1H), 6.72 (d, J = 7.8 Hz, 1H), 2.58 (t, J = 7.6 Hz, 2H), 1.66–1.58 (m, 2H), 1.38–1.24 (m, 6H), 0.94 ppm (t, J = 6.7 Hz, 3H); HRMS-ES+: m/z $[M+H]^+$ calcd for $C_{16}H_{21}N_3O_2$: 288.1712, found: 288.1716; HPLC: t_R = 6.0 min (98% purity).

2-((2-Fluoropyridin-3-yl)oxy)-5-hexylphenol (PT161): A stirred solution of **35** (607 mg, 2.0 mmol) in HF/pyridine (70%, 1 mL) was cooled to −78 °C. After addition of $NaNO_2$ (158.7 mg, 2.3 mmol), the solution was kept at 0 °C for 30 min and then at 60 °C for 1 h. After the reaction was shown to be complete by TLC, the mixture was poured into cold water (10 mL) and neutralized by saturated

aq $NaHCO_3$. The aqueous mixture was extracted with CH_2Cl_2 (2× 10 mL), the organic layer was dried over $MgSO_4$, filtered and concentrated in vacuo to give crude intermediate, which was further treated according to the general demethylation procedure. Purification by flash chromatography (EtOAc/hexane, 15%) gave **PT161** as a light yellow solid (284 mg, 49%): ^{1}H NMR (300 MHz, $CDCl_3$): $\delta = 7.86$ (td, $J = 1.5$, 4.8 Hz, 1H), 7.28 (td, $J = 9.6$, 1.5 Hz, 1H), 7.10 (dd, $J = 4.8$, 7.8 Hz, 1H), 6.91 (d, $J = 2.1$ Hz, 1H), 6.78 (d, $J = 8.1$ Hz, 1H), 6.68 (dd, $J = 2.1$, 8.1 Hz, 1H), 2.55 (t, $J = 7.8$ Hz, 2H), 1.59 (m, 2H), 1.30 (m, 6H), 0.89 ppm (t, $J = 3.3$ Hz, 3H); ^{13}C NMR (75 MHz, $CDCl_3$): $\delta = 155.9$, 152.7, 147.1, 141.4, 140.6, 140.3, 140.3, 140.0, 139.7, 127.5, 127.5, 122.0, 122.0, 120.7, 118.9, 117.0, 35.4, 31.7, 31.3, 28.9, 22.6, 14.1 ppm; HRMS-ES+: *m/z* $[M+H]^+$ calcd for $C_{17}H_{20}FNO_2$: 290.1494, found: 290.1488.

3-(4-Hexyl-2-hydroxyphenoxy)picolinonitrile (PT164): Compound **3** (1.0 g, 4.8 mmol) and 3-bromopicolinonitrile (1.1 g, 5.8 mmol) were reacted according to the same procedure as described for **34** to give **33** as a light yellow solid (0.43 g, 27%): MS (ESI+, 70 eV): *m/z* (%): 311.0 (100), 312.2 (23) $[M+H]^+$. Crude compound **33** was then reacted further according to the general demethylation procedure, and purification of the product by flash chromatography (EtOAc/hexane, 10%) gave **PT164** as a light yellow solid (583 mg, 41%): ^{1}H NMR (400 MHz, $CDCl_3$): $\delta = 8.43$ (d, $J = 4.5$ Hz, 1H), 7.47 (dd, $J = 8.7$, 4.5 Hz, 1H), 7.29–7.28 (m, 2H), 6.94 (d, $J = 7.0$ Hz, 1H), 6.72 (d, $J = 9.0$ Hz, 1H), 5.69 (br s, 1H), 2.61 (t, $J = 7.5$ Hz, 2H), 1.64–1.59 (m, 2H), 1.39–1.33 (m, 6H), 0.91 ppm (t, $J = 6.2$ Hz, 3H); ^{13}C NMR (100 MHz, $CDCl_3$): $\delta = 156.9$, 145.1, 143.7, 143.6,129.0, 128.1, 123.6, 118.8, 118.8, 114.4, 108.0, 107.7, 31.6, 29.9, 22.6, 14.1 ppm; HRMS-ES+: *m/z* $[M+H]^+$ calcd for $C_{18}H_{20}N_2O_2$: 297.1603, found: 297.1607.

Crystallization and structure determination

Crystals of the InhA–NAD^+–**PT119** ternary complex were obtained by the hanging drop, vapor diffusion method.[9] To co-crystallize **PT119**, InhA (5 mg mL^{-1}) was incubated with 2 mM NAD^+ and 2 mM **PT119** in 4% DMSO for 2 h at RT before mixing 1 μL of which with 1 μL of reservoir solution containing 2.4 M sodium acetate (pH 5.0), 200 mM NaCl, 14% PEG 3350 and 4% DMSO. The crystals were allowed to grow for 20 d before soaking in a solution containing 2.8 M sodium acetate, 75 mM NaCl, 21% DMSO, 2 mM NAD^+ and 2 mM **PT119**, and cryo-cooling in liquid nitrogen.

Datasets were collected at the National Synchrotron Light Source at Brookhaven National Laboratory (Upton, New York, USA) on beamline x12c. The reflections were indexed, integrated, and scaled using HKL2000,[21] and structures were solved using MolRep[22] with the crystal structure, taken from the RCSB Protein Data Bank (PDB), of InhA as a model (PDB: 2X23[9]). NAD^+ and **PT119** were built into the difference map calculated from the initial solutions. Structural refinement restraints for NAD^+ and **PT119** were generated using eLBOW.[23] Coordinates and atomic displacement parameter (ADP) refinement including individual atom and correlated anisotropic grouped rigid-body displacement refinement by Translation-Libration-Screw (TLS) parameterization, simulated annealing, and water picking were performed using Phenix.[24] Model building and real-space refinement were performed in Coot.[25] Data collection and refinement statistics are given in Table S2 in the Supporting Information.

The atomic coordinates and experimental data for the crystal structure of InhA–NAD^+–**PT119** have been deposited in the RCSB Protein Data Bank under ascension code 4OIM and are available via http://www.rcsb.org/pdb.

In vivo efficacy

All experiments performed with animals at Colorado State University are conducted under AAALAC approved guidelines and has an OLAW number of A3572-01.

Bacterial strain: The *M. tuberculosis* strain used in the mouse studies was Erdman TMCC 107. Working stocks of bacteria were grown in Proskauer–Beck medium to mid-logarithmic phase growth ($OD_{600} = 0.3$–0.5), dispensed in 1 mL aliquots, and stored at −80 °C. The bacteria used in all the in vivo experiments were from these stocks.

Mouse studies: In vivo efficacy against *M. tuberculosis* Erdman was assessed in the rapid *M. tuberculosis* animal model of efficacy, which utilizes gamma-interferon gene-disrupted (GKO) C57BL/6 mice (Jackson Laboratories, Bar Harbor, ME, USA).[26] Treatment started five days post-infection, with all compounds being delivered via intraperitoneal injection in a formulation of 15% EtOH, 20% propylene glycol, 40% polyethylene glycol 400, phosphate-buffered saline.

Control animals were treated with formulation alone. **PT070** was given 50 mg kg^{-1} BID day 1–4, 25 mg kg^{-1} BID day 5–10, and **PT091** was given 25 mg kg^{-1} BID day 1–4, 12.5 mg kg^{-1} day 5–6, 12.5 mg kg^{-1} SID and 25 mg kg^{-1} SID day 7–10. Animals were sacrificed after 10 days of treatment, and the spleen was homogenized in sterile saline (0.85%) and homogenates were diluted in saline and plated on 7H11 agar supplemented with 10% OADC, 0.01% asparagine, and antibiotics (10 mg L^{-1} cycloheximide, 50 mg L^{-1} carbenicillin).

Bacterial burden in the spleen was determined by enumeration of bacterial colonies after three weeks of incubation. The significance between control and treatment groups was determined via an unpaired, one-tailed t-test (t-test 1,2) with 95% confidence intervals from mean colony-forming units (CFUs) (GraphPad Software ver. 5, San Diego CA USA, www.graphpad.com).

Steady state kinetics and progress curve assays

Kinetic assays using *trans*-2-dodecenoyl-Coenzyme A (DD-CoA) and wild-type InhA were performed as described previously to determine IC_{50} values and residence times.[9,19b] IC_{50} values were determined by varying the concentration of inhibitor in 150 mM piperazine-*N*,*N*′-bis(2-ethanesulfonic acid) (PIPES) buffer containing 250 μM NADH, 25 μM DD-CoA, and 20, 50, or 100 nM InhA. Progress curves were obtained in reaction mixtures containing InhA (5 nM), glycerol (8%, *v/v*), bovine serum albumin (0.1 mg mL^{-1}), DMSO (2%, *v/v*), DD-CoA (300 μM), NADH (250 μM) and inhibitor (0–1000 μM). Inhibition constants for rapid reversible and slow-onset inhibitors were determined using previously reported methods.[9,27] Data fitting was performed using Grafit 4.0 (Erithacus Software Ltd, Horley, UK).

Docking experiments

A model for the complex formed between **PT109** and InhA was obtained using the DOCK 6 suite of programs.[28] The partial atomic charges of cofactor and ligand were computed based on the semi-empirical AM1-BCC[29] method using AMBER 10.[30] The partial atomic charges of amino acids in the protein were assigned based on the AMBER ff99SB force field.[31] The binding site was prepared as described previously.[32] Briefly, a molecular surface for InhA was computed using the program DMS.[33] The program SPHGEN in

DOCK 6 was used to generate a set of spheres at the regions where inhibitor atoms could potentially interact favorably with the receptor. In total, 39 spheres were used to guide inhibitor placement during flexible docking. The grid file was computed with a 0.3 Å grid space using the program GRID in DOCK 6, and default parameters were then used for flexible docking.

Acknowledgements

This work was supported by US National Institutes of Health (NIH) grants AI070383 and GM102864 to P.J.T. Financial support for the National Synchrotron Light Source beamlines x29 and x12c comes principally from the US Department of Energy, Offices of Biological & Environmental Research and of Basic Energy Sciences, and from the US National Center for Research Resources (P41RR012408) and National Institute of General Medical Sciences (P41GM103473), both part of the NIH.

Keywords: diaryl ethers · enoyl-ACP reductases · fatty acid biosynthesis · InhA · inhibitors · structure–activity relationships · time-dependent inhibition

[1] a) H. D. Donoghue, M. Spigelman, C. L. Greenblatt, G. Lev-Maor, G. K. Bar-Gal, C. Matheson, K. Vernon, A. G. Nerlich, A. R. Zink, *Lancet Infect. Dis.* **2004**, *4*, 584 – 592; b) N. S. Shah, A. Wright, G. Bai, L. Barrera, F. Boulahbal, N. Martín-Casabona, F. Drobniewski, C. Gilpin, M. Havelková, R. Lepe, R. Lumb, B. Metchock, F. Portaels, M. F. Rodrigues, S. Rüsch-Gerdes, A. Van Deun, V. Vincent, K. Laserson, C. Wells, J. P. Cegielski, *Emerg. Infect. Dis.* **2007**, *13*, 380 – 387.

[2] *WHO Report 2009—Global Tuberculosis Control: Epidemiology, Strategy, Financing*, publication WHO/HTM/TB/2009.411, World Health Organization, **2009**, http://www.who.int/tb/publications/global_report/2009/en/ (Last accessed: February 21, 2014).

[3] a) T. J. Sullivan, J. J. Truglio, M. E. Boyne, P. Novichenok, X. Zhang, C. F. Stratton, H.-J. Li, T. Kaur, A. Amin, F. Johnson, R. A. Slayden, C. Kisker, P. J. Tonge, *ACS Chem. Biol.* **2006**, *1*, 43 – 53; b) C. Vilcheze, A. D. Baughn, J. Tufariello, L. W. Leung, M. Kuo, C. F. Basler, D. Alland, J. C. Sacchettini, J. S. Freundlich, W. R. Jacobs, Jr., *Antimicrob. Agents Chemother.* **2011**, *55*, 3889 – 3898; c) J. S. Freundlich, F. Wang, C. Vilcheze, G. Gulten, R. Langley, G. A. Schiehser, D. P. Jacobus, W. R. Jacobs, Jr., J. C. Sacchettini, *ChemMedChem* **2009**, *4*, 241 – 248.

[4] a) A. Dessen, A. Quemard, J. S. Blanchard, W. R. Jacobs, J. C. Sacchettini, *Science* **1995**, *267*, 1638 – 1641; b) A. Banerjee, E. Dubnau, A. Quemard, V. Balasubramanian, K. S. Um, T. Wilson, D. Collins, G. de Lisle, W. R. Jacobs, Jr., *Science* **1994**, *263*, 227 – 230.

[5] a) B. Lei, C. J. Wei, S. C. Tu, *J. Biol. Chem.* **2000**, *275*, 2520 – 2526; b) G. S. Timmins, V. Deretic, *Mol. Microbiol.* **2006**, *62*, 1220 – 1227.

[6] M. E. Boyne, T. J. Sullivan, C. W. amEnde, H. Lu, V. Gruppo, D. Heaslip, A. G. Amin, D. Chatterjee, A. Lenaerts, P. J. Tonge, R. A. Slayden, *Antimicrob. Agents Chemother.* **2007**, *51*, 3562 – 3567.

[7] H. Lu, K. England, C. am Ende, J. J. Truglio, S. Luckner, B. G. Reddy, N. L. Marlenee, S. E. Knudson, D. L. Knudson, R. A. Bowen, C. Kisker, R. A. Slayden, P. J. Tonge, *ACS Chem. Biol.* **2009**, *4*, 221 – 231.

[8] a) R. A. Copeland, D. L. Pompliano, T. D. Meek, *Nat. Rev. Drug Discovery* **2006**, *5*, 730 – 739; b) D. C. Swinney, *Curr. Top. Med. Chem.* **2006**, *6*, 461 – 478; c) D. C. Swinney, *Lett. Drug Des. Discovery* **2006**, *3*, 569 – 574; d) P. J. Tummino, R. A. Copeland, *Biochemistry* **2008**, *47*, 5481 – 5492; e) R. A. Copeland, *Expert Opin. Drug Discovery* **2010**, *5*, 305 – 310; f) H. Lu, P. J. Tonge, *Curr. Opin. Chem. Biol.* **2010**, *14*, 467 – 474.

[9] S. R. Luckner, N. Liu, C. W. amEnde, P. J. Tonge, C. Kisker, *J. Biol. Chem.* **2010**, *285*, 14330 – 14337.

[10] C. W. amEnde, S. E. Knudson, N. Liu, J. Childs, T. J. Sullivan, M. Boyne, H. Xu, Y. Gegina, D. L. Knudson, F. Johnson, C. A. Peloquin, R. A. Slayden, P. J. Tonge, *Bioorg. Med. Chem. Lett.* **2008**, *18*, 3029 – 3033.

[11] a) M. Wolter, G. Nordmann, G. E. Job, S. L. Buchwald, *Org Lett.* **2002**, *4*, 973 – 976; b) H. Zhang, D. W. Ma, W. G. Cao, *Synlett* **2007**, 0243 – 0246; c) R. A. Altman, A. Shafir, A. Choi, P. A. Lichtor, S. L. Buchwald, *J. Org. Chem.* **2008**, *73*, 284 – 286.

[12] a) J. J. Niu, H. Zhou, Z. G. Li, J. W. Xu, S. J. Hu, *J. Org. Chem.* **2008**, *73*, 7814 – 7817; b) H. Lang, P. Zoufala, S. Klaib, A. del Villar, G. Rheinwald, *J. Organomet. Chem.* **2007**, *692*, 4168 – 4176.

[13] G. Marsh, R. Stenutz, A. Bergman, *Eur. J. Org. Chem.* **2003**, 2566 – 2576.

[14] a) F. Julémont, X. de Leval, C. Michaux, J. Damas, C. Charlier, F. Durant, B. Pirotte, J. M. Dogné, *J. Med. Chem.* **2002**, *45*, 5182 – 5185; b) D. Galanakis, C. A. Davis, C. R. Ganellin, P. M. Dunn, *J. Med. Chem.* **1996**, *39*, 359 – 370.

[15] a) J. L. Neumeyer, N. Baindur, J. Yuan, G. Booth, P. Seeman, H. B. Niznik, *J. Med. Chem.* **1990**, *33*, 521 – 526; b) L. A. Bigelow, J. R. Johnson, L. T. Sandborn, *Org. Synth.* **1926**, *6*, 16; c) H. Gilman, M. W. Van Ess, D. M. Hayes, *J. Am. Chem. Soc.* **1939**, *61*, 643 – 648.

[16] H. Lu, P. J. Tonge, *Acc. Chem. Res.* **2008**, *41*, 11 – 20.

[17] H.-J. Li, C.-T. Lai, P. Pan, W. Yu, N. Liu, G. R. Bommineni, M. Garcia-Diaz, C. Simmerling, P. J. Tonge, *ACS Chem. Biol* **2014**, *in press,* DOI: 10.1021/cb400896g.

[18] a) D. A. Rozwarski, G. A. Grant, D. H. R. Barton, W. R. Jacobs, J. C. Sacchettini, *Science* **1998**, *279*, 98 – 102; b) M. J. Stewart, S. Parikh, G. P. Xiao, P. J. Tonge, C. Kisker, *J. Mol. Biol.* **1999**, *290*, 859 – 865.

[19] a) R. Rawat, A. Whitty, P. J. Tonge, *Proc. Natl. Acad. Sci. USA* **2003**, *100*, 13881 – 13886; b) S. L. Parikh, G. Xiao, P. J. Tonge, *Biochemistry* **2000**, *39*, 7645 – 7650; c) D. A. Rozwarski, C. Vilcheze, M. Sugantino, R. Bittman, J. C. Sacchettini, *J. Biol. Chem.* **1999**, *274*, 15582 – 15589.

[20] D. C. Swinney, *Curr. Opin. Drug Discovery Dev.* **2009**, *12*, 31 – 39.

[21] Z. Otwinowski, W. Minor, *Methods Enzymol.* **1997**, *276*, 307 – 326.

[22] A. Vagin, A. Teplyakov, *J. Appl. Crystallogr.* **1997**, *30*, 1022 – 1025.

[23] N. W. Moriarty, R. W. Grosse-Kunstleve, P. D. Adams, *Acta Crystallogr. Sect. D* **2009**, *65*, 1074 – 1080.

[24] P. D. Adams, P. V. Afonine, G. Bunkoczi, V. B. Chen, I. W. Davis, N. Echols, J. J. Headd, L. W. Hung, G. J. Kapral, R. W. Grosse-Kunstleve, A. J. McCoy, N. W. Moriarty, R. Oeffner, R. J. Read, D. C. Richardson, J. S. Richardson, T. C. Terwilliger, P. H. Zwart, *Acta Crystallogr. Sect. D* **2010**, *66*, 213 – 221.

[25] P. Emsley, K. Cowtan, *Acta Crystallogr. Sect. D* **2004**, *60*, 2126 – 2132.

[26] a) A. M. Cooper, D. K. Dalton, T. A. Stewart, J. P. Griffin, D. G. Russell, I. M. Orme, *J. Exp. Med.* **1993**, *178*, 2243 – 2247; b) A. J. Lenaerts, V. Gruppo, J. V. Brooks, I. M. Orme, *Antimicrob. Agents Chemother.* **2003**, *47*, 783 – 785.

[27] S. Sivaraman, T. J. Sullivan, F. Johnson, P. Novichenok, G. Cui, C. Simmerling, P. J. Tonge, *J. Med. Chem.* **2004**, *47*, 509 – 518.

[28] P. T. Lang, S. R. Brozell, S. Mukherjee, E. F. Pettersen, E. C. Meng, V. Thomas, R. C. Rizzo, D. A. Case, T. L. James, I. D. Kuntz, *RNA* **2009**, *15*, 1219 – 1230.

[29] a) A. Jakalian, B. L. Bush, D. B. Jack, C. I. Bayly, *J. Comput. Chem.* **2000**, *21*, 132 – 146; b) A. Jakalian, D. B. Jack, C. I. Bayly, *J. Comput. Chem.* **2002**, *23*, 1623 – 1641.

[30] D. A. Case, T. E. Cheatham, T. Darden, H. Gohlke, R. Luo, K. M. Merz, A. Onufriev, C. Simmerling, B. Wang, R. J. Woods, *J. Comput. Chem.* **2005**, *26*, 1668 – 1688.

[31] V. Hornak, R. Abel, A. Okur, B. Strockbine, A. Roitberg, C. Simmerling, *Proteins Struct. Funct. Bioinf.* **2006**, *65*, 712 – 725.

[32] S. Mukherjee, T. E. Balius, R. C. Rizzo, *J. Chem. Inf. Model.* **2010**, *50*, 1986 – 2000.

[33] DMS; UCSF Computer Graphics Laboratory: San Francisco, CA. http://www.cgl.ucsf.edu/Overview/software.html.

[34] Schrodinger, LLC, The PyMOL Molecular Graphics System, Version 1.3r1, **2010**.

Received: October 30, 2013
Published online on March 11, 2014